UNIVERSIDADE ESTADUAL DE CAMPINAS
Faculdade de Engenharia Mecânica

ANDRÉ DANTAS FREIRE

A study of the influence of the microstructure in the micro-milling process

Um estudo da influência da microestrutura no processo de micro fresamento

CAMPINAS

2019

ANDRÉ DANTAS FREIRE

A study of the influence of the microstructure in the micro-milling process

Um estudo da influência da microestrutura no processo de micro fresamento

Dissertation presented to the School of Mechanical Engineering of the University of Campinas in partial fulfillment of the requirements for the degree of master's in mechanical engineering, in the area of Manufacture and Material Engineering.

Dissertação apresentada à Faculdade de Engenharia Mecânica da Universidade Estadual de Campinas como parte dos requisitos exigidos para a obtenção do título de Mestre em Engenharia Mecânica, na Área de Materiais e Processos de Fabricação.

Orientador: Prof Dr. Amauri Hassui

ESTE EXEMPLAR CORRESPONDE À VERSÃO FINAL DA DISSERTAÇÃO DEFENDIDA PELO ALUNO ANDRÉ DANTAS FREIRE, E ORIENTADO PELO PROF. DR. AMAURI HASSUI

CAMPINAS

2019

Ficha catalográfica
Universidade Estadual de Campinas
Biblioteca da Área de Engenharia e Arquitetura
Luciana Pietrosanto Milla - CRB 8/8129

F883s

Freire, André Dantas, 1991-
A study of the influence of the microstructure in the micro-milling process / André Dantas Freire. – Campinas, SP : [s.n.], 2019.

Orientador: Amauri Hassui.
Dissertação (mestrado) – Universidade Estadual de Campinas, Faculdade de Engenharia Mecânica.

1. Microestrutura. 2. Processamento de imagens. 3. Método dos elementos finitos. 4. Fresamento. 5. Anisotropia. I. Hassui, Amauri, 1967-. II. Universidade Estadual de Campinas. Faculdade de Engenharia Mecânica. III. Título.

Informações para Biblioteca Digital

Título em outro idioma: Um estudo da influência da microestrutura no processo de micro fresamento
Palavras-chave em inglês:
Microstructure
Image processing
Finite element method
Milling
Anisotropy
Área de concentração: Materiais e Processos de Fabricação
Titulação: Mestre em Engenharia Mecânica
Banca examinadora:
Amauri Hassui [Orientador]
Daniel Iwao Suyama
Izabel Fernanda Machado
Data de defesa: 29-07-2019
Programa de Pós-Graduação: Engenharia Mecânica

Identificação e informações acadêmicas do(a) aluno(a)
- ORCID do autor: https://orcid.org/0000-0003-3356-9191
- Currículo Lattes do autor: http://lattes.cnpq.br/4569284678639465

UNIVERSIDADE ESTADUAL DE CAMPINAS
FACULDADE DE ENGENHARIA MECÂNICA
COMISSÃO DE PÓS-GRADUAÇÃO EM ENGENHARIA MECÂNICA
DEPARTAMENTO DE ENGENHARIA DE MANUFATURA E MATERIAIS

DISSERTAÇÃO DE MESTRADO ACADÊMICO

A study of the influence of the microstructure in the micro-milling process

Um estudo da influência da microestrutura no processo de micro fresamento

Autor: André Dantas Freire
Orientador: Prof. Dr. Amauri Hassui

A Banca Examinadora composta pelos membros abaixo aprovou esta Dissertação:

Prof. Dr. Amauri Hassui, Presidente
DEMM/FEM/UNICAMP

Prof. Dr. Daniel Iwao Suyama
FCA/FCA-LIMEIRA/UNICAMP

Prof. Dra. Izabel Fernanda Machado
PMR/EP/USP

A Ata da defesa com as respectivas assinaturas dos membros encontra-se no processo de vida acadêmica do aluno

Campinas, 29 de julho de 2019.

DEDICATION

This dissertation is dedicated to my parents who had never failed to give me financial and moral support, for providing everything me what I need in any time to develop my research, and for staying every time by my side to help me when I had difficulties.

ACKNOWLEDGMENTS

First and foremost, to the one above all of us, the omnipresent God, for answering our prayers for giving us the strength to plod on despite our constitution wanting to give up and throw in the towel, thank you so much, Lord.

To the Tool Systems Research Lab in the University of Illinois of Urbana-Champaign with the leadership of Professor Shiv Gopal Kapoor, in collaboration with "School of mechanical engineering-UNICAMP"; sponsored by the department of mechanical science and engineering of UIUC.

I offer our sincerest gratitude to our advisers Amauri Hassui and Shiv Gopal Kapoor, whose encouragement, guidance, and support from the initial to the final level enabled me to develop an understanding of the subject. Without their advice and persistent help, this project would not have been possible.

To my parents, I would like to thank them for supporting me in my daily lives, for going to school every day and having them by my side to guide me always, their prosperity and love for myself.

To Alana Freire, Artur Freire, Priscila Pádua and my all family for always reminding what professional ethics is that made me a better individual, for the advice that they have given to me and their support to me to be global competitive student.

This work could not be completed without the cooperation of several people whom I pay my tribute to:

To Adilson Oliveira, Anselmo Diniz, Aristides Magri, Arnaldo Oliveira, Daniel Suyama, Fabiano Correa, Luciano Barbosa, Rodolfo Zanuto, Rodrigo Lopes, Vanessa Seriacopi.

UIUC Ph.D. students Asif Tanveer and Chi-Ting Lee also collaborated actively in the characterization process performed during the research.

UNICAMP Ph.D. students, Carlos Ancelmo, Gildeones Protázio, Tatiany Mafra, Herbert Aguiar, Marcos Guilherme, Marta Carvalho, Yordan Almeida, Monica Costa

UNICAMP MS. students John Reis, Luiz Ribeiro, Pedro Barbosa, Rener Pontes, Sarah Caldas, Victor Saciotto, Ximena Garcia

Last but not the least, to my American friends who share amazing moments in my master period in USA, Aaron Mccoy, Bruna Scotton, Juan Cruz, Juliana Maia, Larissa Mazuchelli, Lucas Borges, Ludmila Magalhães, Maria Júlia, Mariana Grancieri, Marina Trevisoli, Rafael Campos, Renan Caldas, Roberto Assis, Samuel Rossi, Sinem Güler, Tarik Tanure, Thais Cristina, Umut Uyar.

I want to thank them and everyone whom I did not say here for guiding me and making mine research successful and reliable.

“There are ordinary and extraordinary people. Which one do you want to be? Opportunities are on our way, and we have to be persistent in our goals”

Roberto Carlos Ramos

RESUMO

Existem diversos desafios na criação de microcomponentes pelos processos de microfabricação. Isso porque os microcomponentes, atualmente, são produzidos pelos processos de manufatura aditiva. Como o processo da manufatura aditiva não é perfeito, o pós-processamento passa a ser uma medida necessária após a manufatura aditiva. Para atender as necessidades de pós-processamento são realizadas operações de micro fresamento nesses materiais. Como as micro-operações envolvem uma grande escala nos processos, se faz necessário observar a microestrutura dos materiais durante essas operações. Logo, durante o processo de micro fresamento, os materiais foram submetidos às análises de elementos finitos com as características da microestrutura durante cada simulação. Para isso, foi desenvolvido um programa capaz de identificar e produzir essas características de forma da microestrutura de qualquer material. Com isso, foi desenvolvido um novo método para o mapeamento e aquisição das microestruturas para o desenvolvimento de análises de micro fresamento em software de elementos finitos. O programa inicia o processo com a aquisição de uma imagem bidimensional por meio de técnicas de processamento de imagem para a identificação das fases e definição da microestrutura dos materiais. A criação deste novo método é capaz de gerar malhas com geometrias realísticas a partir de qualquer tipo de microestrutura com formas completamente diferentes. Com a criação destas geometrias é possível diminuir a limitação encontrada em função da interferência humana, e desenvolver um procedimento mais simplificado para o processo de análise. Uma análise dos comportamentos de micro fresamento foi realizada em um software de elementos finitos a fim de se observar a diferença entre dois materiais. Onde uma análise considerou um material com as características da microestrutura, e a outra considerou sem a microestrutura. Os materiais estudados foram definidos com base nas diferentes geometrias e na quantidade de fases encontradas nas microestruturas. Por fim, ensaios de micro fresamento foram realizados em mesmo material produzido por um processo de manufatura aditiva com a variação do ângulo de deposição. Esses ensaios foram realizados a fim de se observar a influência das propriedades de usinagem do micro fresamento em relação às diferentes camadas da manufatura aditiva. Com a variação do ângulo de deposição do material da manufatura aditiva, o material começou a apresentar características de anisotropia durante o processo de micro fresamento. Portanto, foram encontrados os esforços de corte durante o micro fresamento a fim de se determinar a estratégia mais adequada para processo e comprovar a anisotropia do material da manufatura aditiva durante o processo de microusinagem.

Palavras chave: Microestrutura, Processamento de Imagem, Elementos Finitos, Micro Fresamento, Camadas de Deposição, Anisotropia.

ABSTRACT

There are several challenges in the creation of micro components by micro-manufacturing processes. Besides, micro components are currently produced by the additive manufacturing processes. Considering the process of additive manufacturing is not perfect, post-processing becomes a necessary measure after additive manufacture. Also, the micro-milling operations are performed on these materials to satisfy post-processing requirements. As micro-operations involve a large scale in the processes, it is necessary to observe the microstructure of the materials during these operations. Thus, during the micro-milling process, the materials were subjected to the analysis of finite elements with the characteristics of the microstructure during each simulation. For this, the software was developed capable of identifying and processing these shape characteristics of the microstructure of any material. On this, a new method was finished for the mapping and acquisition of microstructures for the development of micro-milling analysis in finite element software. The program starts the process with the acquisition of a two-dimensional image using image processing techniques for the identification of the phases and definition of the microstructure of the materials. The creation of this new method is capable of generating meshes with realistic geometries from any type of microstructure with entirely different shapes. With the creation of these geometries, it is possible to reduce the limitation found in the function of human interference and to develop a more simplified procedure for the analysis process. An analysis of the micro-milling behavior was carried out in finite element software in order to observe the difference between two materials. One analysis considered a material with the characteristics (shapes) of the microstructure, and the other considered with no microstructure. The studied materials were defined based on the different geometries and the number of phases found in the microstructures. Finally, micro milling tests were carried out on the same material produced by an additive manufacturing process with the variation of the deposition angle. These tests were carried out in order to observe the influence of the machining properties of the micro-milling concerning the different layers of the additive manufacture. Among the variety of the deposition angle of the material of the additive manufacturing, the material began to present anisotropy characteristics during the micro-milling process. Therefore, the cutting efforts were found during micro-milling in order to determine the most proper strategy and to prove the anisotropy of the material of the additive manufacture during the micromachining process.

Keywords: Microstructure, Image processing, Finite elements, Micro-milling, Deposited layers, Anisotropy.

LIST OF ILLUSTRATIONS

LIST OF TABLES

LIST OF ABBREVIATIONS AND ACRONYMS

2D	Two dimensional
3D	Three dimensional
AM	Additive manufacturing
ASTM	American society for testing and materials
EBM	Electron beam melting
FE	Finite element
FEM	Finite element method
fig	Figure
n	Number of homogeneous materials
png	Portable network graphics
PSD	Pattern Standard Deviation
jpeg	Joint photographic experts group
RMS	Root Mean Square
SEM	Scanning electron Microscopy

LIST OF EQUATIONS

SUMMARY

1 INTRODUCTION

Several steps characterize the process of manufacturing any material up to the final production of a product. Also, the manufacturing process had undergone several technological advances, and it had added many technologies in progress. The manufacturing process has long been related to concepts of subtractive and formative manufacturing. However, through the various technological advancements in these areas, it began to incorporate the additive manufacturing terminology into the manufacturing processes (BROOKES, 2014; YOON et al., 2014).

The concepts of subtractive and formative manufacturing are related to the processes with chip formation and no chip formation respectively. Subtractive processes can be turning, milling, drilling, grinding, water jetting, abrasive blasting, abrasive flow, and ultrasound. The formative processes are those of casting, welding, powder metallurgy and forming (rolling, extrusion, drawing, forging and stamping). Consequently, additive manufacturing arose because of the need to improve and update manufacturing processes by significantly transforming existing models (ZHU et al., 2013).

With many technological advances, the demand for manufacturing of miniaturized components began to increase, which are responsible for several segments of society. Besides, the amount of materials that can be used in these processes is growing every day. One of the main problems related to the manufacturing process, on a micro scale, is related to the significant challenges of the scale effect because the tools present considerable challenges in the miniaturization, in the impact of the minimum chip layer or the geometric characteristics of the grains in the microstructure of the materials (GHERMAN et al., 2017).

The identity of the materials is characterized by the geometry and structure of the grains in the microstructure. However, the changes present in the microstructure can significantly influence mechanical properties (BABU et al., 2016; TESSEMA et al., 2017). In micro machining, the influence of the mechanical resistance is quite noticeable, making it fundamental to consider its geometry, shape, and size. Besides, the study of process models using the microstructure of the material promotes a better understanding of the mechanical, thermal and microstructural interactions (PAN; FENG; LIANG, 2017).

The miniaturization of the components is an application widely used in micro milling processes. Besides, micro milling technology is commonly applied in aviation, microelectronics, micro-optics, military, manufacturing of implants, medical and dental prostheses (BREME et al., 2016; CHENG; HUO, 2013; MAHAPATRO, 2015; QU et al., 2017). Also, the additive manufacturing processes are geared towards applications with a lot of technology, from aerospace to personal care; however when seeking high quality, post-processing is required for example with micro milling (SALONITIS et al., 2016). The post-processing is used for the correction of some unwanted characteristics in the piece (SAMES et al., 2016).

Since the micro-milling processes present several difficulties due to the complexities of the operations, and these challenges were widespread to use programs for finite element calculations. Since micro milling tools have a maximum diameter of one-millimeter, finite element programs are used to understand the micro-milling process. The micro-milling presents results, cutting mechanisms and dynamics very different from conventional ones (e.g. meso and macro milling) (ÖZEL; OLLEAK; THEPSONTHI, 2017; THEPSONTHI; ÖZEL, 2016).

The idea of finite element methods comes from the need to solve complicated problems at one time. Although the finite element method does not guarantee a perfect result, currently there are specific mathematical tools that can approach the results to real life. These results can explain the most diverse applications in practical problems. Besides, it is possible to improve the effects of a finite element analysis more and more as we spend more on computational efforts (RAO, 2018).

Various types of materials can be used in additive manufacturing operations. The titanium, aluminum, tool steels, superalloys, stainless steel and refractory are the most commonly used commercially materials (FRAZIER, 2014). The materials used in the micro-milling processes by additive manufacturing are quite varied in their applications. As these quantities of materials are quite diverse, the process of the investigation will be described generically for any king of material. The main interest will be to understand the mechanical stresses due to the microstructure and anisotropy of the materials. For this, two scopes of work will be addressed in this research:

- Generation and characterization of the microstructure for a finite element software; and
- The analysis and comparison of finite elements of the micro-milling of materials with homogeneous and heterogeneous microstructure.

1.1 General objective

The overall objective of this research is to create a new method for the generation of a mesh with realistic geometries of the microstructure for various types of materials. Consequently, the efforts involved in a finite element analysis with a workpiece with microstructure and no microstructure were analyzed.

1.2 Specific objectives

For achieving the overall goal of this research, it is necessary to achieve the following specific objectives:

- Examine the impact in micro-milling finite element analysis of a material with the microstructure shapes and no microstructure shapes (characteristics);
- Define the best method to do the micro-milling in a finite element software;
- Formulate a mesh to finite element analysis with a realistic shape of the microstructure grains; and
- Develop a method to create the microstructures from bidimensional image to a finite element software.

1.3 Researches importance

The importance of this research is related to the development of studies related to micro processes, such as micro milling. The main factors associated with this process, such as the microstructure of the material were analyzed. For those as mentioned earlier, two questions were considered: Does the microstructure of the materials influence the analysis of finite elements during micro-milling? And, does there any method for automatically acquiring the microstructure of any material without operator interference?

2 LITERATURE REVIEW

This chapter shows the theoretical background for the knowledge of the new method for the micro-milling analysis of two different kinds of materials which has completely different shapes considering the microstructure characteristics in the finite elements. For this, the processing of images to acquire microstructures is explained; the influence of microstructures on finite elements; the anisotropy of materials. In all the explanations are shown studies carried out in the literature.

2.1 Image processing for acquisition of the grains

The creation of a 2D mesh for the analysis of finite elements for a microstructure from a two-dimensional image is a process that demands many steps and challenges. This is because most types of materials do not present an utterly homogeneous microstructure, with different shapes and sizes of grain. The irregularity on the microstructural grains can make the process for creating realistic geometric models of the microstructure and meshes for finite element analysis quite complicated (NADIMI et al., 2015; WANG; KWAN; CHAN, 1999; YANG et al., 2018). So, the microstructure is composed of atomic arrangements that form the grain regions. I.e., the microstructure is the single-phase grains of metals with different sizes and shapes of microconstituents. They are usually found within arrangement/morphology in a multiphase system (METALS., 2018; SANTOS, 2006). The diversity of the geometries of each microstructural grain disrupts the creation of the mesh because the meshes were created with polygons (KIKINZON; SHASHKOV; GARIMELLA, 2018). Moreover, when a mesh of a given microstructure was created with polygons, this mesh cannot describe the whole grain shape. Therefore, the grains were not defined by primitive methods.

The process of image acquisition, whether they are two-dimensional or three-dimensional, was primarily differentiated by two methods, “X-ray computed tomography” and “metallographic processes” (NICOLETTO; ANZELOTTI; KONEČNÁ, 2010). This enabled the analysis of the meshes in a 3D or 2D, respectively. However, most programs involve the manual processes, with user intervention to do image processing, further, the manual method is time-consuming. In order to solve the problem of automating the grain selection process in the material microstructure, DeCost and Holm (2015) created a program capable of differentiating the various types of materials such as bronze, brass, ductile cast iron, gray cast iron, hypo eutectoid steel, malleable cast iron, superalloy, among others. Although it is an automated program to identify the microstructure of different materials, it is not yet a program capable of selecting the different types of grains of each microstructure.

Currently, the program “OOF: Finite Element Analysis of Microstructures” is one of the most used for image processing and mesh creation (LANGER; FULLER; CARTER, 2001; NIST, 2015). However, despite its being easy to use, it is challenging to represent the FE meshes with shapes characteristics of the grains realistically in the microstructures. Many authors have explored other programs for the creation and analysis of finite element meshes (BARRETT et al., 2018; GOKHALE; YANG, 1999; NADIMI et al., 2015; NICOLETTO; ANZELOTTI; KONEČNÁ, 2010; ZHOU et al., 2015; ZHU et al., 2018). However, these mesh-creating programs have difficulty in dealing with the microstructure of the material consisting of the irregular grain structure of grain boundaries. Recently, Barret et al. (2018) created grains with triangular meshes that caused an improper form of the grains on the surface of the voxels (elementary unity at the three-dimensional space). They used a surface correction filter to suppress these irregularities (BARRETT et al., 2018). Besides, the authors claimed that the research is not valid to find mechanical behavior correctly when grain morphology was ignored. Since the images can contain many noises, they can hinder the characterization of the boundaries regions of each grain. Therefore, in manual processes of image characterization, experienced operators are fundamental to the correct identification of each area (CAMPBELL et al., 2018).

The overall goal of this step is to create a mesh for “FEM” by mapping automatically. The objective is to outline a microstructure through image processing for the creation of a mesh for finite element analysis. This is done to avoid the microstructure variables such as geometry, shape, and size, interfering with a final examination. To solve the problem of mesh generation with the realistic microstructures of each image a method is developed to select the grain of the microstructures automatically. Besides, the coordinates for each pixel are generated in an orderly manner, to create a structure for the creation of the meshes. To make the process of acquiring the image and creating meshes for the analysis of finite elements to be more straightforward and more inexpensive a method has been developed that creates three-dimensional structures with SEM images. The method of acquisition and processing image, with the creation of ordered points, following by the creation of the structures continuously for the creation of the meshes can be seen in the flowchart of Figure 1. In Section 3 of this work, the processes found in this flowchart will be detailed.

Figure 1 - Flowchart for creation of the meshes

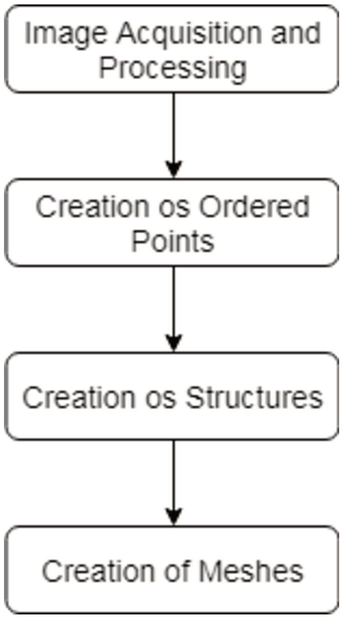

2.2 Influence of microstructure in a finite element

The microstructure of the material can significantly influence the process of manufacturing and analysis of the same because the characteristics of these are generally not homogeneous (ARISOY; ÖZEL, 2015; NADIMI et al., 2015). Since micro milling is considered a scale down of a conventional milling process, this process presents many issues of operationalization (THEPSONTHI; ÖZEL, 2015). In general, the operations are entirely applied in the manufacture of matrices and molds, electronic sensors, biomedicine, aviation, among others (GOK et al., 2017; JIN; ALTINTAS, 2012).

The study about the influence of the microstructure into materials as well as their use in finite element software is significant for the micro-milling process. This is because of factors such as size effect, tool edge radius, ploughing, can significantly influence mechanical stresses and promote tool wear (AHMADI et al., 2018). The grain size, the microstructure, and the machining performance can be evaluated through numerical simulations based on finite elements (ARISOY et al., 2016).

The phenomena that influence the microstructure of the chip formation materials, as well as the surface effects, have been investigated by several authors. Pu et al. (2016) investigated the changes that the morphology of the chip variations with the increase of the cutting speed, considering the holes in the microstructure of steel 1045. It was included that the morphology of the chip can change from continuous to discontinuous and serrated as the events occur in the microstructure in the zone of shear with increasing cutting speed. Besides these, Arısoy and Özel, (2015) studied the effects of surface integrity on machining processes in the Ti-6Al-4V material microstructure, where the grain size and the microstructure of the material were brought to the finite element software for the operations of conduction of temperature, stress, ploughing and strain rate to be analyzed. Other researchers have used finite element methods to solve problems with chip formation in micro milling, heat and temperature distribution phenomena, and calculation of shear forces (THEPSONTHI; ÖZEL, 2015).

2.3 Material anisotropy

For some materials from additive manufacture, the anisotropy is a property of the material that depends on the orientation of growth of the layers in its microstructure. This orientation is related to the directions where the mechanical, electrical, thermal, among other properties will occur. The anisotropy properties are usually restricted to boundary conditions that are related to the symmetry of the materials (KOCKS; WENK; TOMÉ, 1998).

The anisotropic characteristics were first recognized in metallic and rocky materials by Halloy in 1833 where layers of different depositions of the material have received the terminology of textures (WENK; HOUTTE, 2004).

Unlike anisotropic materials, the isotropic materials present very similar mathematical calculations when compared to ordinary applications. It is worth noting that the main difference between these materials is related to the variation of effort (VINSON; SIERAKOWSKI, 1986).

Generally, characteristics such as mechanical stress, and thermal, physical and electrical properties cannot be found in anisotropic materials when analyzed in a specific coordinate axis. Due to these characteristics, several elements are arranged in sets so that some traits are added to obtain more satisfactory results. For example, in some beams (where there are concrete and steel parts) of civil construction, rebars (ferrous material) are placed in a specific direction so that the applied loads are supported. If these loads were applied differently, the beam would lose its main characteristic of support (VINSON; SIERAKOWSKI, 2002).

As in civil construction, composite materials with established microstructures are quite common in everyday life. In electrical aspect, it was tried to develop methods to measure the resistivity of anisotropic materials. This resistivity is responsible for micrometric variations which interfere a system as a whole (MONTGOMERY, 1971).

3 METHODOLOGY

This chapter describes the definitions for the design and elaboration of a methodology for the acquisition and processing of images with microstructures, with the ordering of each element in the mathematical matrix, with the creation of structures and meshes. Besides, the mechanisms for characterization of the microstructure used in this work will be expressed. The chapter also explains which was the finite element software, tool, machine tool, and experimental planning, used for the micro-milling process. This structure can be found in the Project Flowchart at the end of the chapter.

3.1 Image acquisition and processing

The acquisition process of a realistic microstructure for any material begins with the metallographic methods that are responsible for ensuring an excellent characterization of the material analyzed. After the metallographic process is concluded, some workpiece with the microstructural grains should be chosen for acquired the image through an optical microscope (MCNAMARA; DIFILIPPANTONIO; RIED, 2005). Figure 2 represents the flowchart of the image acquisition and processing process in this research.

Figure 2 - Flowchart of the image acquisition and processing process

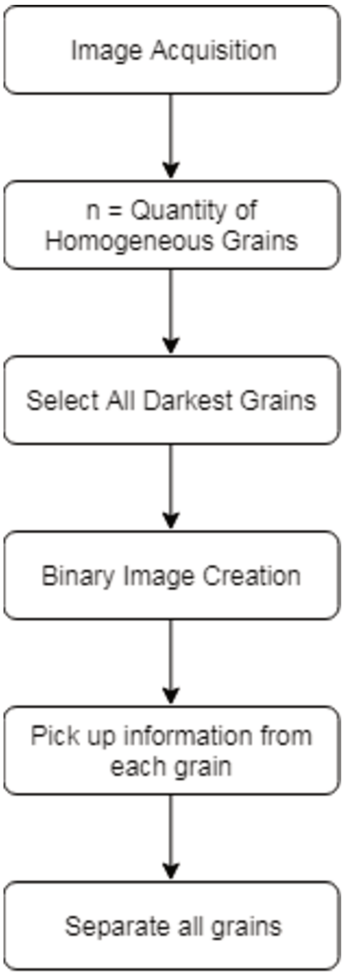

The image processing starts with the choice of a program capable of performing numeric calculations on the saved data packet in a digital format, and this program should be able to perform an iterative analysis of matrices with direct calculations (MATHWORKS, 2018). After the process of choosing the program, it is necessary to inform the number of homogeneous materials "n" present in the microstructure of the material. The number "n" determines the number of cycles in the program. Then, the image processing begins with the acquisition of the microstructure extracted from the optical microscope. This image is saved in any digital format, "jpeg", "png", "fig", among others. Besides this, a matrix $k_{r,c,3}$ is created, where "K", "r", "c" and "3" represent the matrix, rows, columns and the number of layers respectively. These layers are related to the dimensional of the matrix. Every matrix of the image represents a data structure known as pixel or voxel, two-dimensional and three-dimensional data format, respectively. These data structures are stored in sets of mathematical matrices where they can be divided into a value from 0 to 255 (GUEVARA et al., 2003;

RUSS, 2011). Several equations can then be applied to datasets to improve their image characteristics obtained previously (TANIMOTO, 2012).

The grains in the microstructure image are selected using the “Flood Fill” technique, where specific coordinates are established to select a pixel. Moreover, the area was demarcated in the neighborhood of this pixel according to the intensity of the values of each (THE MATHWORKS, 2016). This type of technique can identify and select all the pixel values that were around a coordinate supplied to the system. Region selection occurs as a flood of the regions adjacent to the selected pixel (BURGER; BURGE, 2016; WAYALUN et al., 2012). In Figure 3, it is possible to observe that a pixel is selected and from the value obtained therein, the region to its surroundings is selected.

Figure 3 – (a) Representation of a pixel structure; (b) Representation of a chosen pixel; and (c) Representation of a selected region

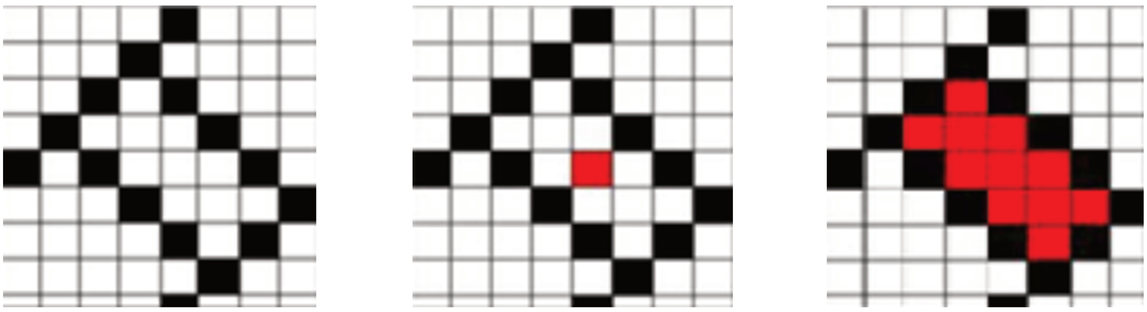

(a) (b) (c)

Figure 3a represents a possible grain structure, Figure 3b represents the chosen matrix element, and Figure 3c represents the flooding process. In this examination, a pixel will be selected within a darker region in the original image of the microstructure, and therefore, the grain will be elected.

The collection of the region of each grain in the microstructure occurs with the calculation of the measurements of the distance of each pixel from the original one, considering the distance of each. The norm $N$of the region needed to perform the calculation can be found in the surroundings of the selected pixel by the following Eq. 1 where N_{ij}^2 denotes the square of each element of “M” matrix.

$$N = \sum_{i=1}^{r}\sum_{j=1}^{c}\sum_{k=1}^{3} N_{ij}^{2} \qquad \text{Eq. 1}$$

Following the calculation of the norm in Eq. 1 and Eq. 2, the matrix must be converted to a grayscale format.

$$N_{ij} = \left(M - M_{ij}T\right)_k \qquad \text{Eq. 2}$$

To equate the value of each weight, a different function is used to calculate the weights for each pixel, based on grayscale intensity difference. The Eq. 3, Eq. 4 and Eq. 5 are showing the matrixes and vector necessary to estimate the norm in Eq. 2.

$$M = \begin{bmatrix} x_{11} & x_{12} & \cdots & x_{1c} \\ x_{21} & x_{22} & & x_{2c} \\ \vdots & & \ddots & \vdots \\ x_{r1} & x_{r2} & \cdots & x_{rc} \end{bmatrix} \qquad \text{Eq. 3}$$

$$M_k = \begin{bmatrix} x_{11k} & x_{12k} & \cdots & x_{1ck} \\ x_{21k} & x_{22k} & & x_{2ck} \\ \vdots & & \ddots & \vdots \\ x_{r1k} & x_{r2k} & \cdots & x_{rck} \end{bmatrix} \qquad \text{Eq. 4}$$

$$x_{ij} = \left(x_{ij1}, x_{ij2}, x_{ij3}\right) \qquad \text{Eq. 5}$$

"T" denotes the all-ones matrix with order $r\ x\ c$, this matrix can be seen in Eq. 6.

$$T = \begin{bmatrix} 1 & 1 & \cdots & 1 \\ 1 & 1 & & 1 \\ \vdots & & \ddots & \vdots \\ 1 & 1 & \cdots & 1 \end{bmatrix} \qquad \text{Eq. 6}$$

Once the norm calculation process was completed with the weight of each pixel next to the original, a region is selected. The selected region was stored in an array in the program itself in a binary format where all the pixels that were selected from that first grain are cataloged. After this step, the process was repeated, the program selected all grains and the entire binary matrix was produced. With the creation of a binary matrix, it was necessary to perform some steps, such as:

- Corrode the ends of the grain;
- Fill with regions or holes; and
- Find the perimeter of each grain in the binary matrix.

Figure 4 represents the image processing methodology for obtaining a matrix/image binary. After processes of grain selection and creation of the binary matrix with all the grains were finalized, the process of identification of each grain began.

Figure 4 – (a) Representation of selected Region; (b) Representation of matrix/image binary.

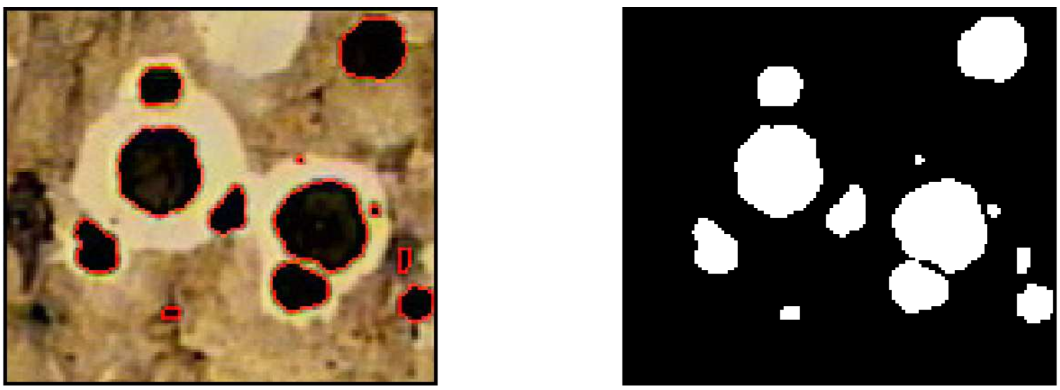

(a) (b)

After the processing in Figure 4, it is possible to extract all the information of each grain, as well as, size, area, cartesian position, among others. Each grain of the image was manipulated independently, so a loop was created with the maximum number of regions in the binary image. Additionally, it was used as a function to find the maximum amount of grains present in the binary matrix and all components of a two-dimensional binary image were cached in a different matrix. Subsequent, the moment the maximum amount of grain was obtained, the process for separating each one was promoted.

All elements of a two-dimensional were stored in a separate matrix. When the moment the maximum amount of grain was obtained, the process for separating each one was facilitated. Moreover, another loop was applied to create a binary image for each grain. This step is to ensure that dimensions, orientations, and positions of the grain were respected.

3.2 Creating ordered points

After the separation of all the grains in their respective binary matrices, it is necessary to find the perimeter of each grain. Although it sounds like a simple operation, this process is quite complex because first of all, the grain may have a structure filled with irregularities as seen in Figure 5.

Figure 5 - Representation of irregular surface a grain in binary format

Produced by an author

Second, if the perimeter is saved in a programming language format (from left to right, top to bottom), the process of generating the structures is impaired. To illustrate the case, Figure 6 illustrates the issue of the contour (the red part) of the grain in the blue insert and the original storage sequence of each pixel. It is possible to see, with the red part, the sequence was not sorted, and something had to be done to correct this ordered problem.

Figure 6 - Original grain boundary sequence

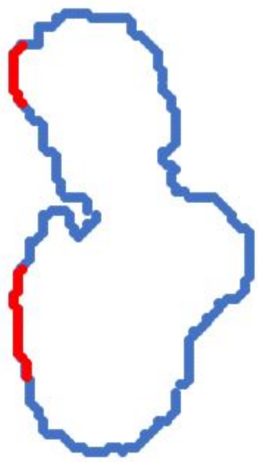

In order to solve this contour condition of the perimeter creation, a program was developed capable of traversing all the edge of the grain respecting its form. The ordering program of the coordinates begins with a copy of the edge of the binary image of the grain "*n*" (as can be seen in Figure 7, the beginning of the procedure is performed finding edges in a binary image. Next, all indexes and non-zero values of the edge copy elements are saved. An array of zeros is created to store the coordinates in the correct order, and the first element of the indexes and non-zero values is added. After that, the binary image distance transform is calculated to identify which is the closest pixel. This distance is found with the aid of the Euclidean distance.

Figure 7 - (a) Represent a microstructural example of a grain; (b) Represent a binary part of it; (c) Representation of orderly contour of this grain part 1; (d) Representation of orderly contour of this grain part 2; (e) Representation of orderly contour of this grain part 3; and (f) Representation of orderly contour of this grain part 4.

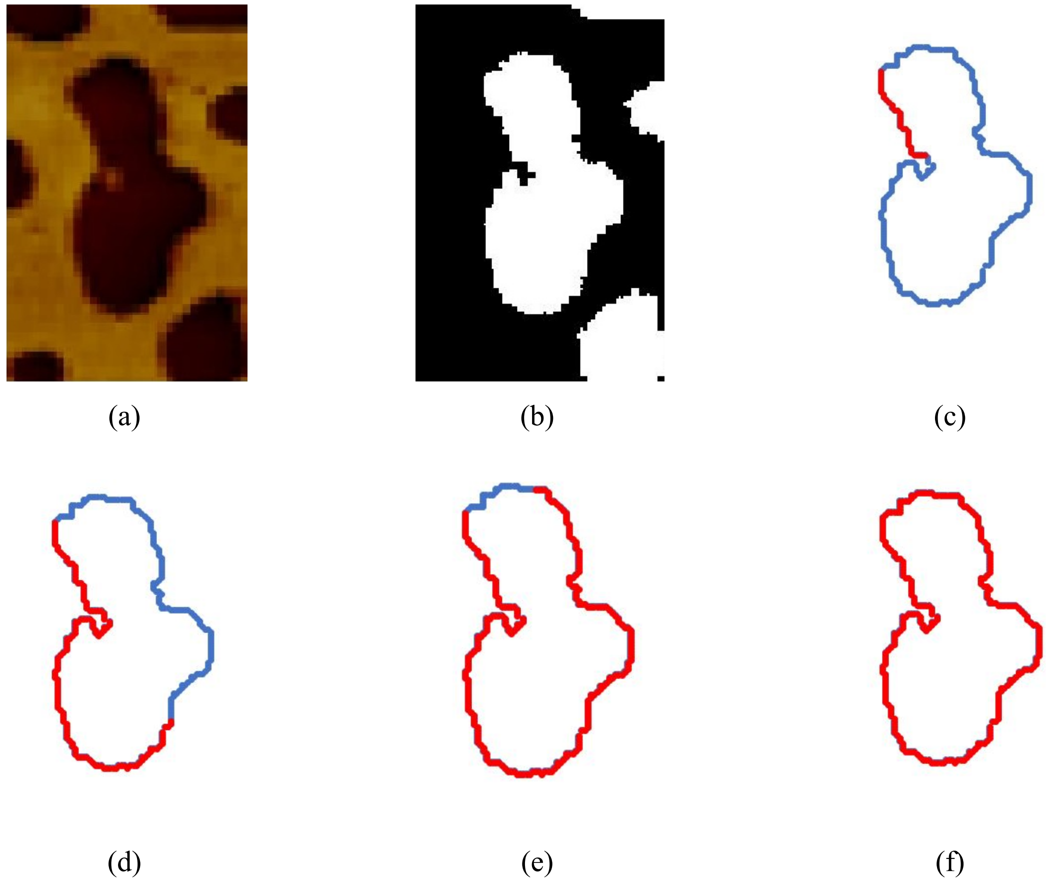

The old values of the edge coordinates are replaced by values ordered in the same binary matrix of the grain, and a file is created with the respective information of each grain. This file is filled with the ordered coordinates that represent the positions of each pixel in the image in the "x" and "y" planes.

3.3 Creation of grain's structures

The creation of the grain's structures starts with the acquisition of the file that was generated in section 3.2. This process was split into three processes: coordinate import, curve creation and extrusion of structures (PTC, 2017).

(a) The point's coordinates were created with datum points offset, where it creates the points in the program work area;
(b) The curve was created by interpolating all coordinates points. Hence the importance of obtaining the ordered points; and
(c) The creation of the extrusion is done after the curve has been created these curves will be extruded, and they represent the realistic shape of each grain.

Considering a material with two characteristics of different materials (n = 2) and that the first region of the grains was extracted by image processing, the second region can only be detected with “Boolean operations”. This complementary method can also be applied to materials with n >= 3. “Boolean operations” are also joint in many modeling software, which characterizes this operation as complementary and this operation is not described in detail over here. This is because these operations were not a necessary resource, but an option for creating the microstructure.

3.4 Creation of meshes

The next step is to create the mesh for the analysis of finite elements after the creation process of each grain structure is completed. Besides this, a standard for the exchange of products model data was created (“step” or “stp” file) file. Therefore, it can be opened in a different modeling program to create the mesh.

For the creation of the mesh, the same modeling software can be used to generate a file in “step” or “stp” format. Later, after some necessary adjustments, the two-dimensional structure was created, and the mesh could be developed with the most natural grain. Every element in the mesh creation has an association with the grain size, and this association never will be less than one, because every nodal element needs to be unitary. An example of the creation of meshes in microstructures with hexahedral elements can be seen in Figure 8.

Figure 8 - Representation of meshes in the microstructure of the material

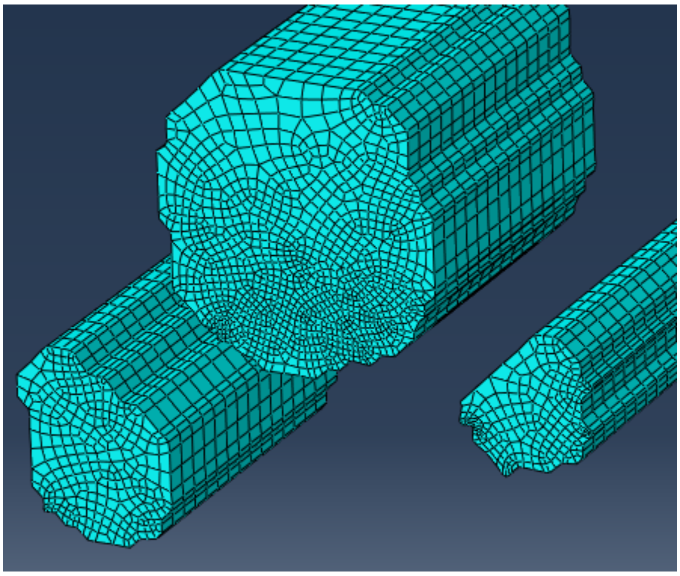

3.5 Finite Element Modeling of orthogonal micro-cutting and parameters

The finite element model for an orthogonal micro-cut was developed with ABAQUS/CAE 2017. Dynamic, explicit and adiabatic conditions were used in the material to guarantee the shortest period with the most considerable plastic deformation during the machining process (SIMULEON, 2018).

The parameters for micro-milling used in this research were based on finishing operations. The axial depth of cut was defined as 100μm, and the radial depth of cut was chosen as 5μm, 10μm, 15μm, and 20μm, respectively. The spindle speed of the micro mill was 16000rpm, and the feed rate was 150mm/min. The radial depth of cut has a constant initial value, but it changes as a function of the movement of the cutting tool. Figure 9 shows the representation of the micro milling tool and the workpiece of nodular cast iron.

Figure 9 – Representation of micro milling process

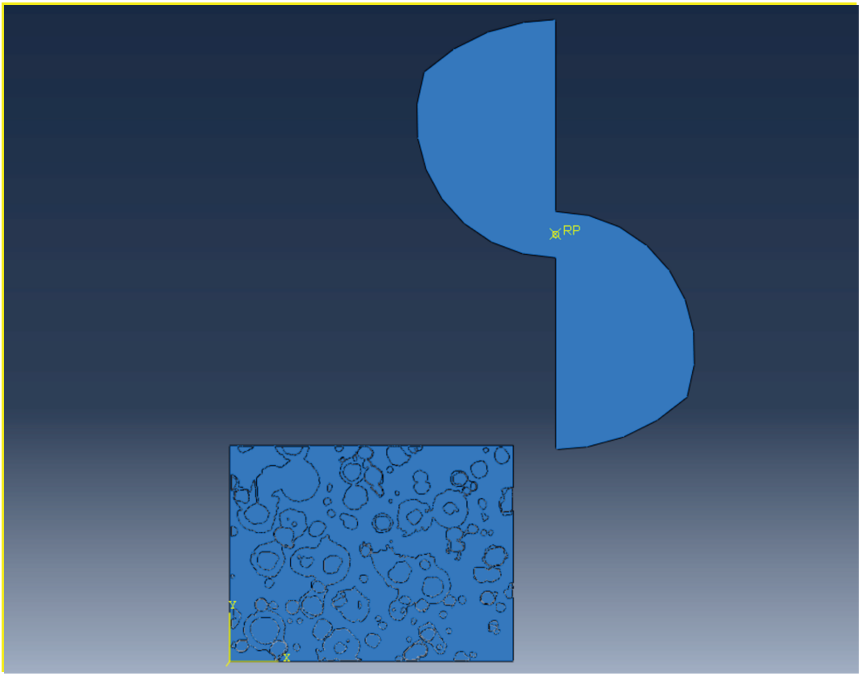

Modeling for finite element analysis was divided into two steps. In the first step, the material used for the research was chosen as nodular cast iron with dimensions of 240µm by 138µm. The second step is related to the selection of machining parameters. The diameter of the micro mill tools can range from 25microns to 1.0mm with flute length of up to 10mm and cutting edge radius from 1 to 20 microns (JIN; ALTINTAS, 2012). A micro mill based on BMS-020-2 of Micro100 was chosen. The diameter of the tool was 508µm, with flute length of 762µm and overall length of 38.1mm. The micro mill also has a rake angle, relief angle, helix angle and radius of 10°, 30° and 30°, respectively.

The mesh of the piece with the microstructure was created with the distance of each pixel used in the microstructure (with a 0.622µm distance between its elements), and it has 91622 elements. The cutting tool consists of 175 elements. All surfaces of each grain in the microstructure used in the piece were constrained with Tie type to ensure perfect contact between them. The cutting tool was restricted with the Rigid Body type option. Besides, a reference point was created in the region of the center of the cutting tool for the acquisition of mechanical stress during the process. All interactions between tool and material were performed between the surfaces of each bead and the mechanical constraint formulation used was penalty contact method, because it aims to approximate the hard pressure-overclosure behaviors. This contact method was chosen to achieve equal force throughout the tool penetration process in the workpiece.

As the manufacturing process analyzed in this research involves a great deal of distortion and rupture (orthogonal cut), it was chosen to create meshes with hexahedral elements to overcome this difficulty. The tetrahedral elements can be less accurate than hexahedral when it is integrating the shape functions with points of Gauss.

3.6 Determination of material data

The model chosen for analysis of stress-strain behavior in the material was that of Johnson-Cook. This model was defined by Eq. 1 (JOHNSON; COOK, 1983).

$$\sigma = (A + B\varepsilon^n)\left(1 + C\, ln\frac{\dot{\varepsilon}}{\dot{\varepsilon}_0}\right)\left[1 - \left(\frac{T - T_r}{T_m - T_r}\right)^m\right] \qquad \text{Eq. 7}$$

Where A represents yield stress (MPa); B is hardening modulus (MPa); ε is the plastic strain; n is the hardening coefficient; C is the strain rate coefficient; $\dot{\varepsilon}_0$ is a reference plastic strain (0.001s-1); T and T_m represent the temperature of the material workpiece (°C) and the melting temperature of the material workpiece (°C) respectively; T_r represents room temperature (RT)(°C); and m is the thermal softening coefficient. The Johnson-Cook parameters extracted from Johnson and Cook (1983) and Chen et al. (2018), and are shown in Table 1.

Table 1 - Johnson-Cook parameters of Nodular Cast Iron

	A[MPa]	**B[MPa]**	**C**	**n**	**m**	**Tm[°C]**	**Tr[°C]**
Graphite	125	400	0.032	0.155	0.9	4000	20
Pearlite	514	1900	0.079	0.26	1.03	1750	20

Adapted from (LJUSTINA; LARSSON; FAGERSTRÖM, 2014).

Parameters of density, Young's modulus, Poisson’s ratio, conductivity, specific heat and inelastic heat fraction are shown in Table 2 and Table 3.

Table 2 - Material properties of Graphite

Property	Materials information
Density [kg/m3]	2560
Young’s modulus [GPa]	25
Poisson’s ratio	0.2
Specific heat [J/kg°C]	837

Adapted from(LJUSTINA; LARSSON; FAGERSTRÖM, 2014).

Fatigue damages, characterized by significant stress disturbances or strain, are functions that relate physically significant variables and it can change the parameters (LEE et al., 2012).

Table 3 - Material properties of Pearlite

Property	Materials information
Density [kg/m3]	7850
Young’s modulus [GPa]	190
Poisson’s ratio	0.3
Specific heat [J/kg°C]	452

Adapted from (LJUSTINA; LARSSON; FAGERSTRÖM, 2014).

In this research the criterion of JC damage was used, and Eq.2 express this.

$$\bar{\varepsilon}_f = \left[D_1 + D_2 exp\left(D_3 \frac{P}{\bar{\sigma}}\right)\right]\left(1 + D_4 \, ln \frac{\dot{\varepsilon}}{\dot{\varepsilon}_0}\right)\left[1 + D_5\left(\frac{T - T_r}{T_m - T_r}\right)\right] \quad \text{Eq. 8}$$

$\bar{\varepsilon}_f$ is the measured FIS (initial strain or strain strain) at specific condition, D_1, D_2, D_3, D_4 and D_5 are material-dependent fracture constants, P is the equivalent compressive stress at specific condition, $\bar{\sigma}$ is the equivalent stress, $\dot{\bar{\varepsilon}}_0$ is the reference strain rate and $\dot{\bar{\varepsilon}}$ is the strain rate at the specific condition. In Table 3, the Johnson-Cook failure parameters used in this work are given.

Table 4 - Johnson-Cook damage coefficients of nodular cast iron

JC damage coefficients		Graphite	Pearlite
Initial failure strain	D1	0.2	0.2
Exponent factor	D2	0.6	0.6
Triaxiality factor	D3	3	3
Strain rate factor	D4	-0.02	-0.04
Temperature factor	D5	0.6	0.6

Adapted from (LJUSTINA; LARSSON; FAGERSTRÖM, 2014)

3.7 Materials used

For the creation of microstructure material's mesh for the analysis of finite elements, two materials with heterogeneous structures were chosen. The first material was perlite nodular cast iron, with three different compositions (ferrite, perlite, and graphite), and the second material was tungsten carbide and cobalt (WC-Co) hard metal with two different compositions. In both materials, metallographic procedures were performed to ensure high-grade visualization of the microstructure (DIETERMANN & HEUSER SOLUTION GMBH, 2018; ROA et al., 2015). Also, two different kind of materials were selected to analyze de code used to produce the microstructure workpiece to FE analysis. These two materials were titanium alloy and undetermined cast iron.

For the simulation of the micro-milling of materials with heterogeneous microstructure, a finite element software was adopted. Toward assure the repeatability of the software used to create the meshes in the microstructures, a new workpiece material was chosen. This material chosen for analysis had an amount of n=3. Consequently, nodular cast iron was selected for this step.

4 RESULTS

In this section of the research results obtained with the acquisition and processing of the microscopic images of each material, and subsequent creation of the structures and meshes for analysis of finite elements will be explained. Therefore, it is important to consider the amount "*n*" of homogeneous materials present in the material image. As already mentioned in the previous session, materials with three and two different structures were chosen in their composition. Suddenly, was analyzed the differences between a material with microstructure and no microstructure in a micro-milling process. Additionally, micro-milling experiments had been conducted to understand the influence of the material deposition layer into the micro-milling process. In the next sections, results for each microstructure will be explained.

4.1 Method for process the microstructure with $n = 2$

A material with two distinct phases ($n = 2$) in its microstructure was a tungsten carbide-cobalt hard metal insert, as can be seen in Figure 10(a). It is also possible to identify a difference in the tonality of the microstructure regions, where one presents a lighter shade, composed of several tungsten carbide grains that promote a high hardness of the material and the second region is a darker shade made up of cobalt binders. The phenomena in the formation process of the carbide insert will not be explained here but can be found in Diniz; Marconde and Coppini (2014).

Figure 10 - (a) Representation of microstructure of a WC-Co carbide insert; (b) Representation of selected region of the WC-Co microstructure; (c) Representation of cobalt grains selected by the program; and (d) Representation of binary Image of the Cobalt Struct

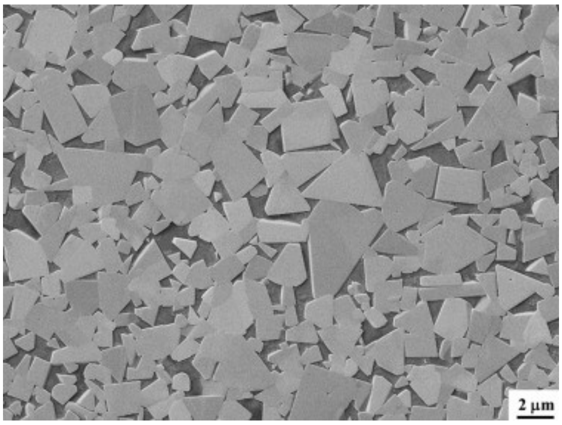

(a)

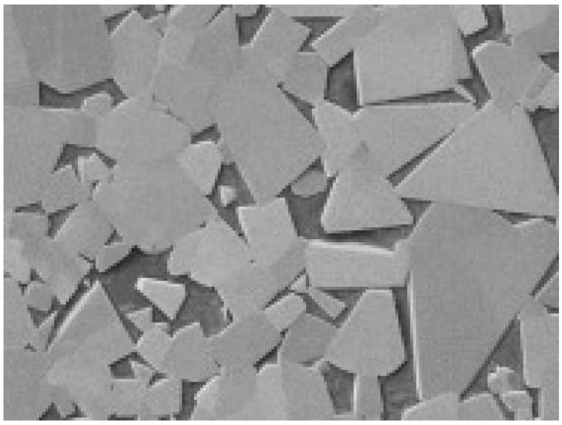

(b)

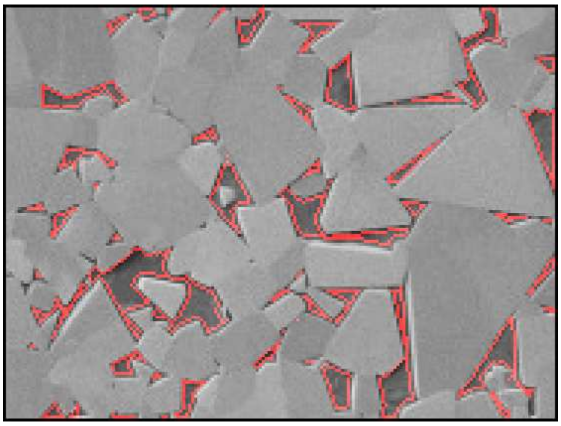

(c)

(d)

From the basic understanding of which structures are present in the microstructure of Figure 10(a), a region was selected to for image processing. This selected region was corresponding microstructure of the material during the behavior analysis. Figure 10(b) shows the region selected for analysis.

After select each cobalt grain regions present in the microstructure of the tungsten carbide-cobalt material, the darker hue pixels were selected. The process was repeated until all cobalt grains were chosen. Figure 10(c) shows the selection of each grain in the microstructure. Following the steps, the binary image forming process is performed so that all the grain information can be extracted. The binary image can be seen in Figure 10(d).

4.2 Method for process the microstructure with *n* >= 3

A material with the amount of *n* >= 3 has a characteristic of at least three distinct materials in its microstructure. Besides this, the process can be reproduced for any material with n bigger than three. The perlite nodular cast iron, displayed in Figure 11(a), will be the material with *n* = 3 used in this work. By examining the microstructure of this material, it is possible to observe three different similar structures were found in darker, lighter color intensity and a medium color scale. The grains characterized by the darker color are grains of graphite, formed by the movement and agglomeration of carbons in the process of solidification of the materials. With the process of carbon agglomeration in the structure of the cast iron, the iron particles were expelled from these regions, thus forming the lighter structures, known as the ferrite region. At the end of the cast iron solidification process, only the intermediate staining regions, where the perlite structures, were located (SANTOS, 2006).

Figure 11 - (a) Representation of microstructure of perlite nodular cast iron; (b) Representation of selected region of the microstructure of perforated nodular cast iron; (c) Representation of grains of graphite selected by the program; (d) Representation of binary image of graphite structure; (e) Representation of process for eliminating graphite grains; (f) Representation of color inversion to select ferrite and graphite grains; (g) Representation of ferrite and graphite grains selected by the program; and (h) Representation of binary image of graphite and ferrite Structure.

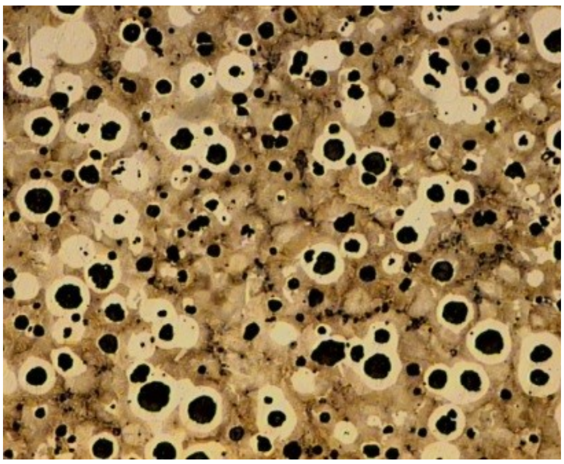

(a)

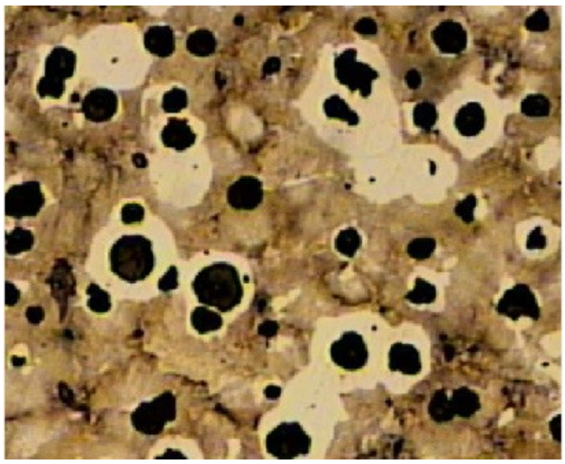

(b)

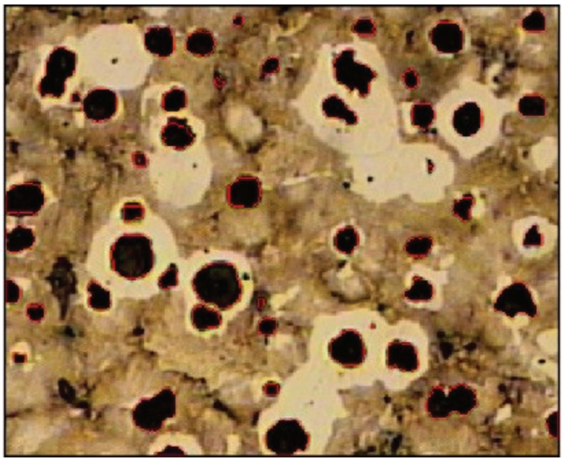

(c)

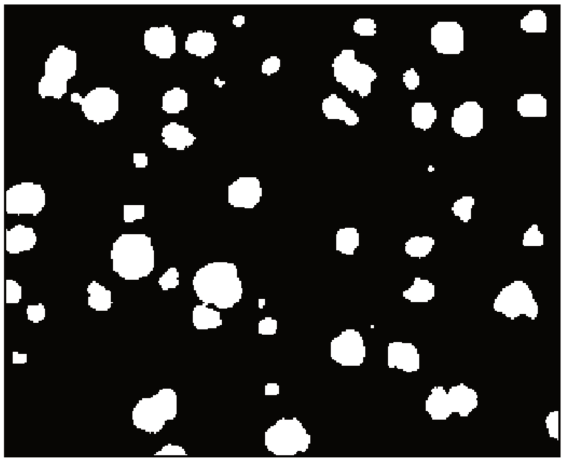

(d)

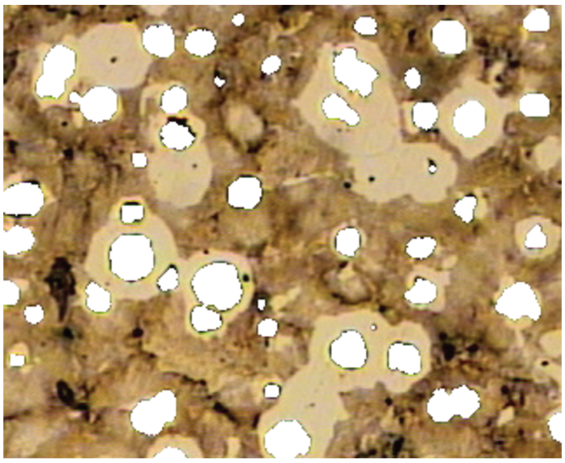

(e)

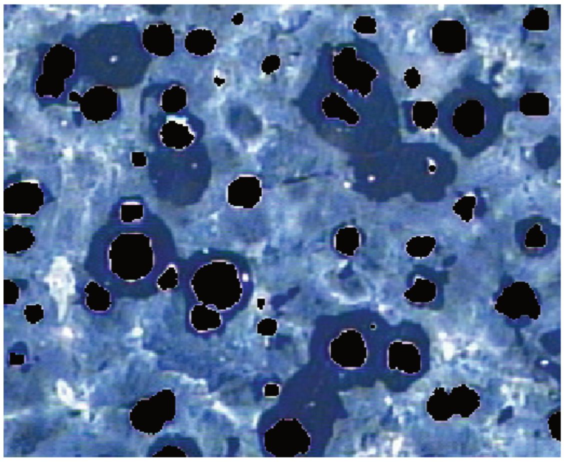

(f)

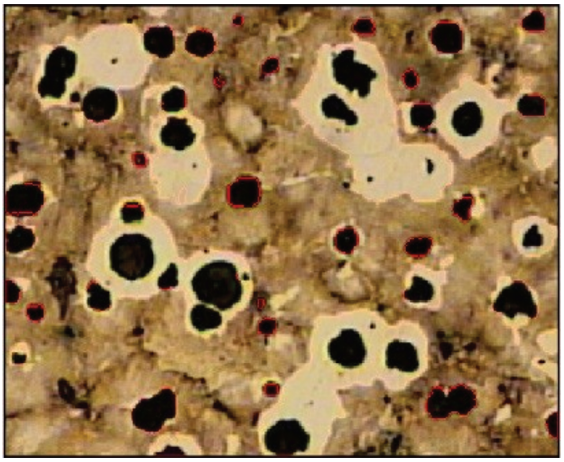

(g)

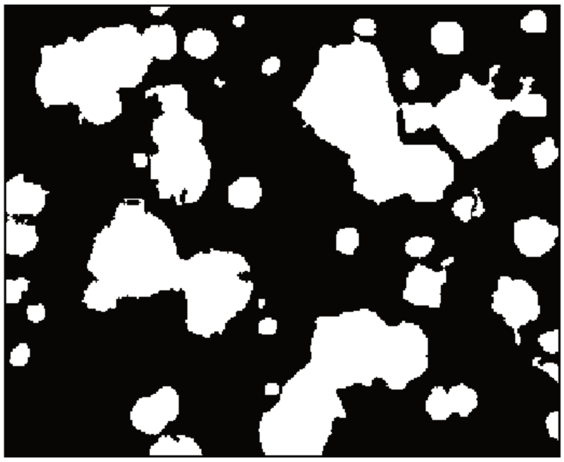

(h)

Similarly, a region of Figure 11(a) was selected for processing the microstructure present in the material. Figure 11(b) shown exactly the region chosen. A windows region was used to select one part of the microstructure with more detail, and then an image processing was performed to obtain the microstructure of the material in a binary format.

Darker hue pixels were selected for image processing. After this step, the region of the selected grains will turn into a binary region. Figure 11(c) and Figure 11(d) shows the regions selected of the grains and the corresponding binary image of each one, respectively.

After completing the selection of the first set of grains, acquisition of the second set of grains of the same microstructure was started. The method for selection of the second region of homogeneous grains is the same as that of the first region. However, a technique excluding the first grains was applied. This technique can be used for all cases of materials with $n >= 3$, with three or more different structures, such as the case of perlite nodular cast iron. A procedure with subtraction of matrices was used to facilitate the removal of the first grains of the microstructure. This simple technique was not explained in the methodology of this work. Figure 11(e) shows the microstructure without the presence of graphite grains in its microstructure.

As the microstructural acquisition program works preferentially with regions of darker hue, a technique for shade inversion of the microstructure was applied. Figure 11(f) shown the result of this technique. The acquisition process of the second set of grains in the microstructure was repeated. It is possible to select the ferritic region of this iron; this region can be seen in Figure 11(g).

Finally, a binary matrix containing the selected region was created; this matrix can be seen in Figure 11(h). It is worth noting that, in the creation of the second region of the microstructure the graphite and ferritic regions were selected. However, they will be separated in the section 4.3.

4.3 Method for creating the microstructures

The end of the image processing, a file with the coordinates point was created. The modeling software imported these. For the creation of each structure, files with the "*x*" and "*y*" coordinates were imported into an offset coordinates system. The location of the coordinate system was chosen and maintained until the end of the process for the same materials. If the same coordinate systems were not used, the grain position could be changed, so it is essential to define the coordinate system because this makes finite element analysis imprecise. A curve was created passing through all points with an interpolation. Then, the structure of each grain was created, and a structure was done. In order to improve the results in the analysis of the finite element meshes, the height of this extrude must have a specific value (KIM; HAFT-JAVAHERIAN; CASTRO, 2016).

Figure 12(a) depicts the creation of the cobalt structures extracted from the WC-Co microstructure. One rectangle must be created to find the tungsten carbide region of the respective microstructure. Accordingly, this rectangle with the same dimensions of "*x*" and "*y*" of the selected microstructure was created as a structure. Besides this, a "Boolean operation" was performed to remove the cobalt material from the rectangle. Therefore, a chrome structure identical to the original one was performed. This microstructure can be seen in Figure 12(b).

Figure 12 - (a) Representation of cobalt structure formed by CREO PARAMETRIC; (b) Representation of structure formed by the tungsten carbide grains; (c) Representation of graphite structure formed by CREO PARAMETRIC; (d) Representation of structure of graphite and ferrite formed by CREO PARAMETRIC; (e) Representation of ferrite structure formed by CREO PARAMETRIC; and (f) Representation of perlite structure formed by CREO PARAMETRIC.

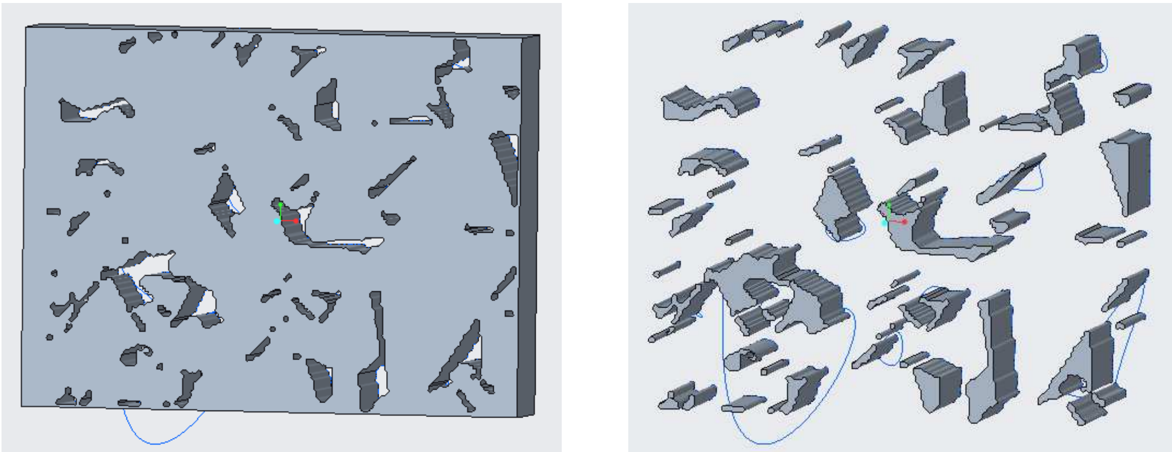

(a) (b)

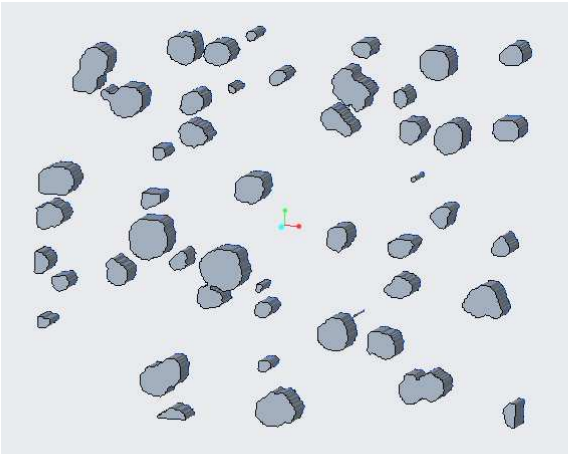

(c)

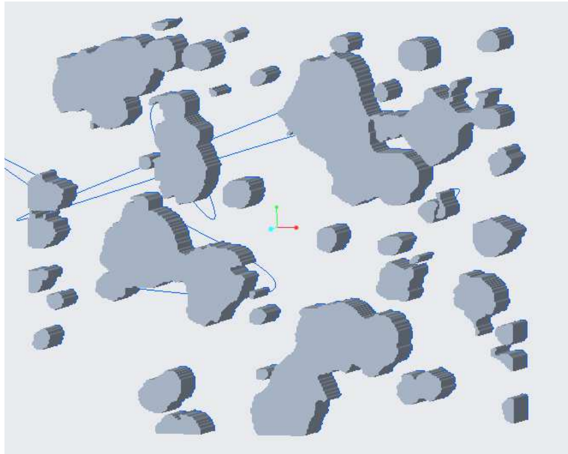

(d)

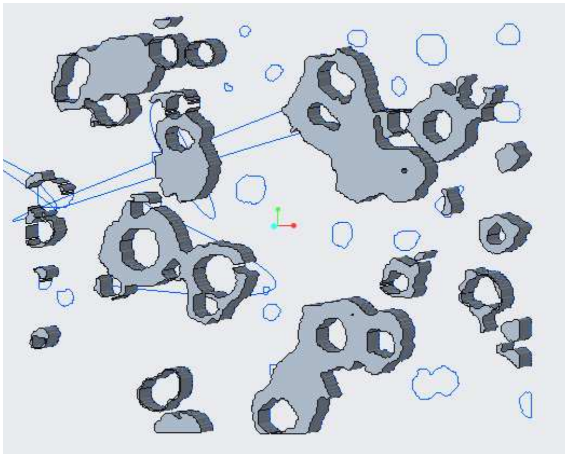

(e)

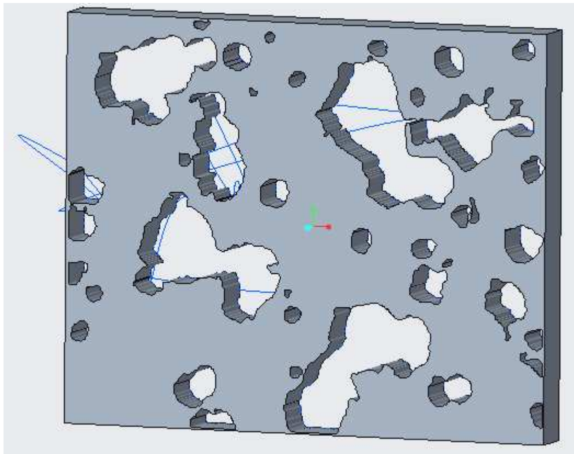

(f)

Concerning the creation of the perlite nodular cast iron structures (material with "n = 3"), the same processes were carried out. Figure 12(c) shown the first region of graphite grains. Suddenly, a structure was created with the graphite and ferritic regions of this material, which was expressed in Figure 12(d). In order to find the region of the ferrite only, a "Boolean operation" was carried out between the graphite and ferrite structures, and the structure of only graphite. Figure 12(e) shown only the structure of ferrite grains. Finally, to find the perlite region (intermediate staining), another "Boolean operation" was performed between a parallelepiped with the dimensions of the selected microstructure, with the graphite and ferrite grains structures. Figure 12(f) shows the structure of the pearlitic region of the microstructure of these materials.

4.4 Method for create the meshes

The concluding process of acquisition of microstructures through the processing of two-dimensional images and the creation of meshes for the subsequent analysis of finite elements, was done when a file was created for each structure. The characteristics for creating each mesh can be changed manually by the operator and must follow the technical procedures (SIMULEON, 2018). A more straightforward illustration for some parts of Figure 12 was used to create the meshes in Figure 13(a) and Figure 13(b). The structures of WC-Co can be found. Figure 13(c) represents the structural assemblies of each material like that previously stated.

Figure 13 - (a) Represents a zoom of Co meshes; (b) Denotes a zoom WC meshes; and (c) Describes the zoon assembly of WC-Co.

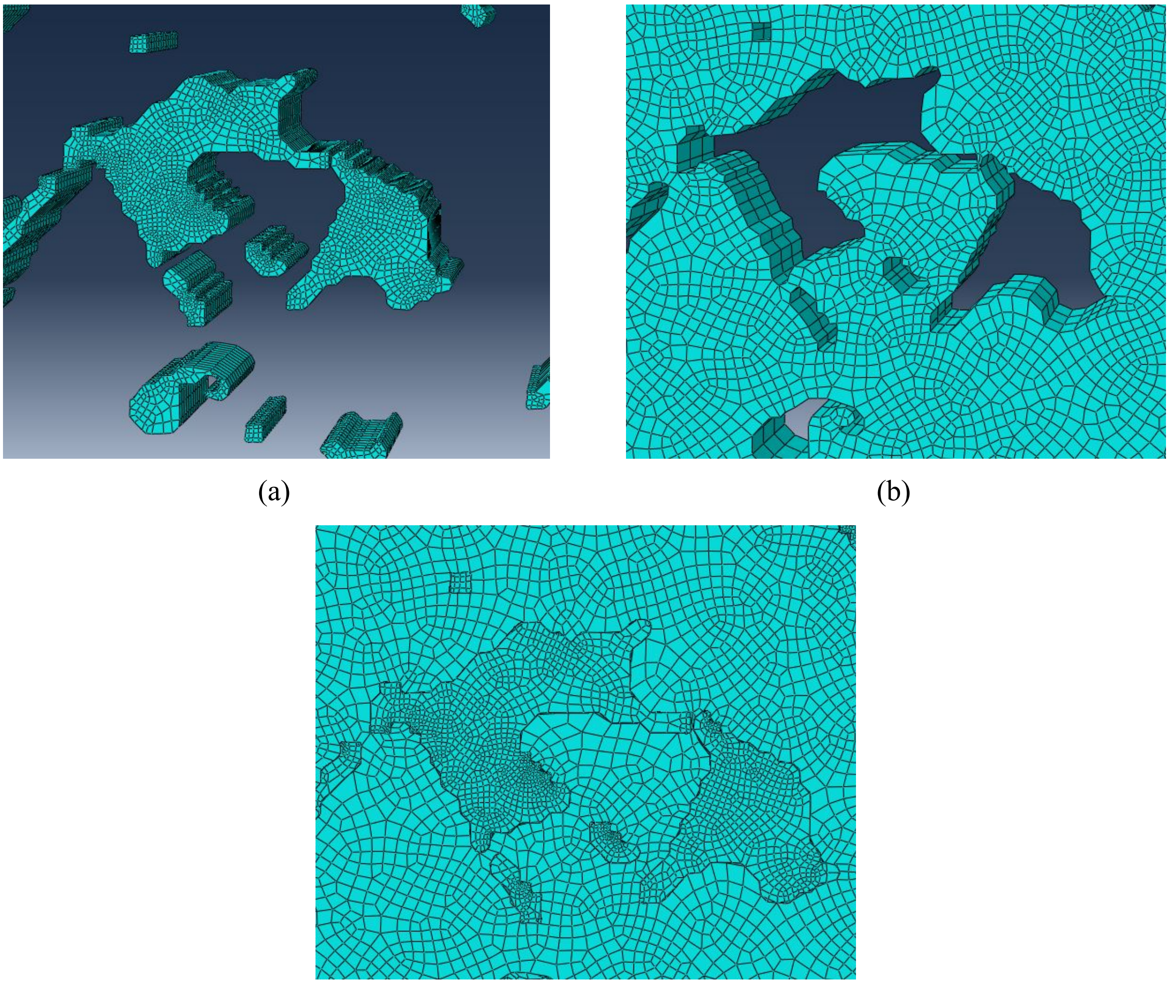

(a) (b)

(c)

As was done for WC-Co, the structures of perlite nodular cast iron can be seen in Figure 12. Figure 14(a) shows an example of a graphite grain; Figure 14(b) shown the structure of the ferrite; Figure 14(c) was shown the third element, the pearlite. The assembly process with all meshes is shown in Figure 14(d).

Figure 14 - (a) Represents a zoom of graphite meshes; (b) Denotes a zoom ferrite meshes; (c) Describes a zoom of Perlite meshes; and (d) Expresses the assembly part of all Nodular Cost Iron meshes.

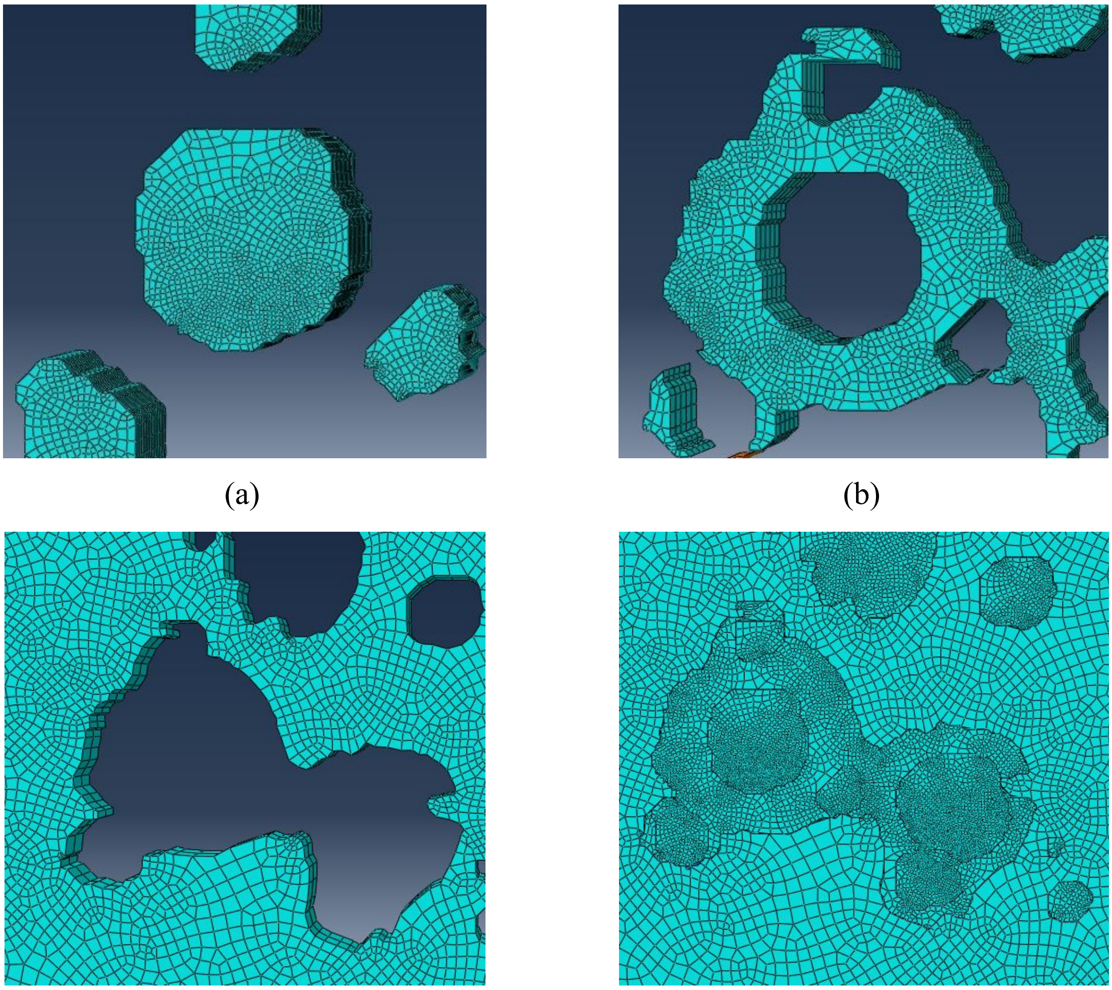

(a) (b)

(c) (d)

4.5 Additional materials used

Two different materials were used to express how accurate the program of imaging processing is. Also, it is an essential detail of the extreme differences in these materials. The first material was a titanium alloy, and the second was undetermined cast iron. These imaging processing can be seen in the Figure 15.

Figure 15 - Additional images processed. (a) original titanium alloy; (b) image processed of titanium alloy; (c) original undetermined cast iron; and (d) image processed of undetermined cast iron.

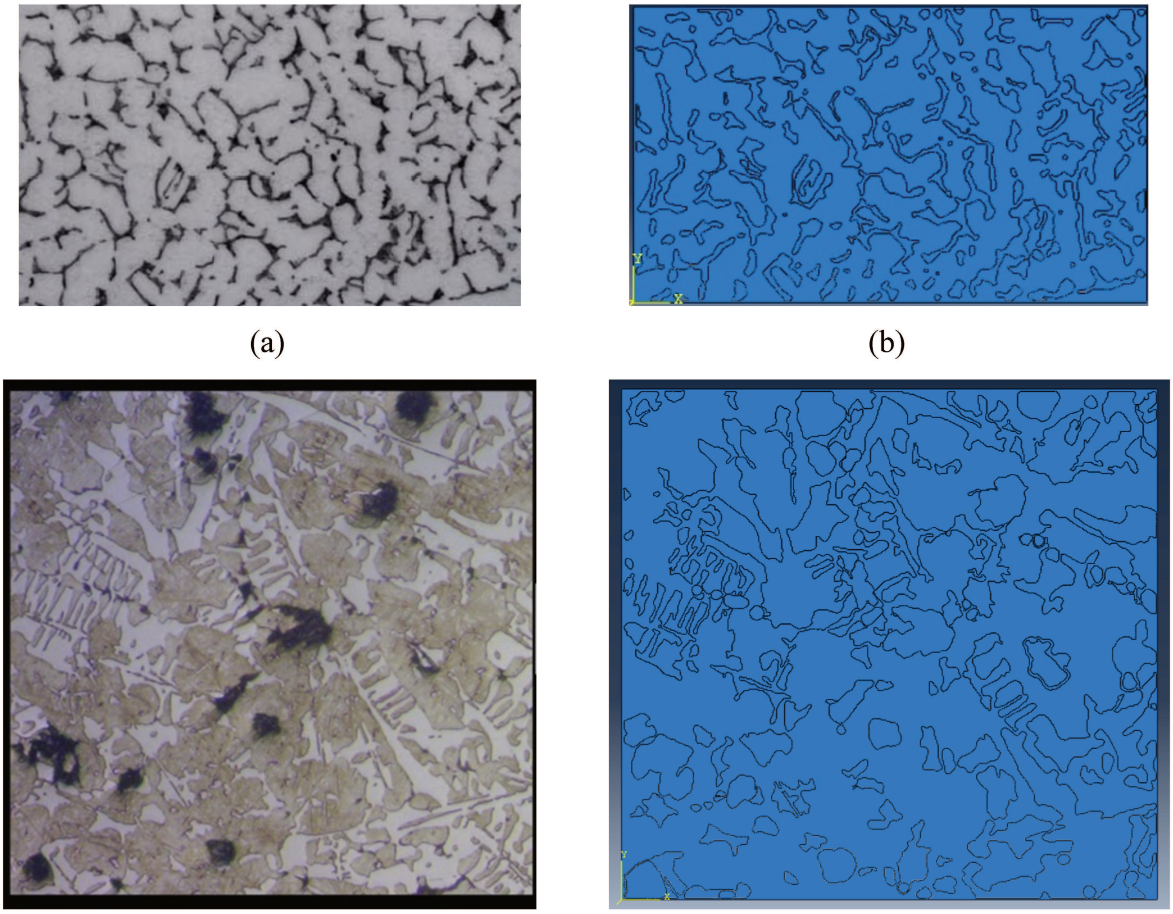

(a) (b)

(c) (d)

4.6 Simulation of micro-milling FE

The simulations of micro-milling FE with microstructures were applied to the identification of the influence between grains in the structure of Nodular Cast Iron and the micro mill tool, Figure 9. Although the phases of each material have different characteristics in their microstructures, it was essential to point out these different phases of the materials interfere with the micro-machining process with a much more significant factor in comparison with macro machining.

Finite element analyses were performed on two part's models — one with the determined microstructure and a different one with no microstructure. Data acquisitions were made to start the discussion. Figure 16(a) had shown the relationship between forces on the x-axis between the material with defined microstructure and material with no defined microstructure. In this illustration, the x-axis represented the mechanical forces in the direction perpendicular of the feed direction. Furthermore, the y-axis represents the mechanical behaviors in the direction of the feed direction. All stress forces were expressed in Newtown. It was observed the root mean square (RMS) was higher for the workpiece with microstructure in cases of 5µm, 10µm and 15µm radial depth of cut. In this case, the variation as a function of the microstructure in the workpiece represented 72%, 33%, and 11%, respectively. However, the workpiece without microstructure remained larger in the RMS of "*x*" only for the case of the radial cut depth of 20µm. The analysis made it in Figure 16 of any quest that a workpiece with microstructure had longer forces than another one with no microstructure in the workpiece.

Figure 16 - RMS behaviors (a) x; (b) and y.

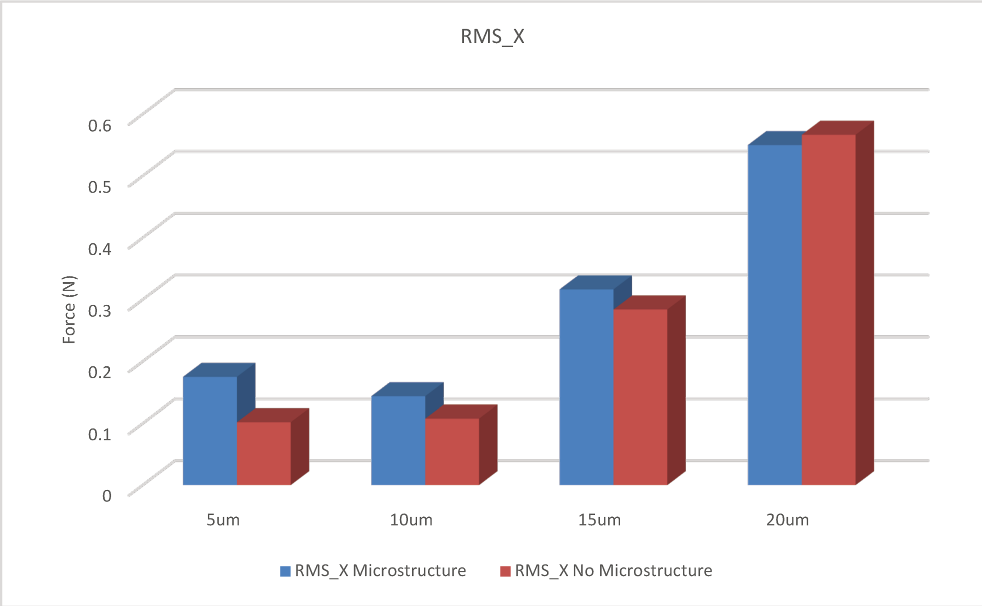

(a)

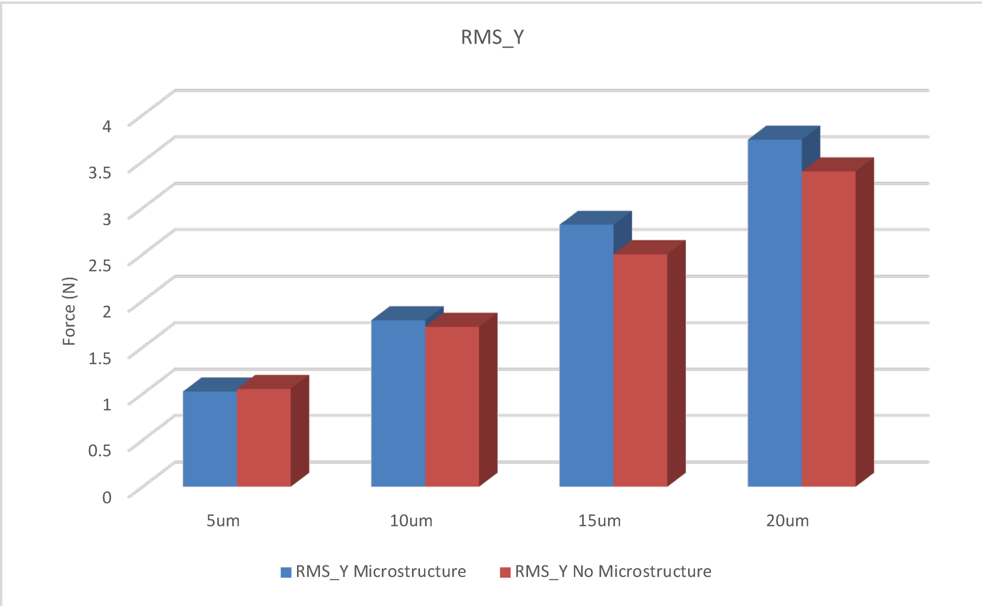

(b)

For the forces on the y-axis, Figure 16(b), the results were very similar to those on the x-axis, where practical, all the results of the mechanical stresses on the x-axis remained higher than the y-axis. The workpiece without microstructure showed a small increase during the cut of 5µm of the radial cut depth of 3% regarding the workpiece with microstructure. However, for the radial depth of cut with 10µm, 15µm and 20µm, the workpiece with microstructure presented 4%, 13%, and 10% increase about the workpiece without microstructure. Figure 17(a) shows these differences between the RMS forces.

Figure 17 - (a) Difference of error between x and y forces; (b) and pattern standard deviation

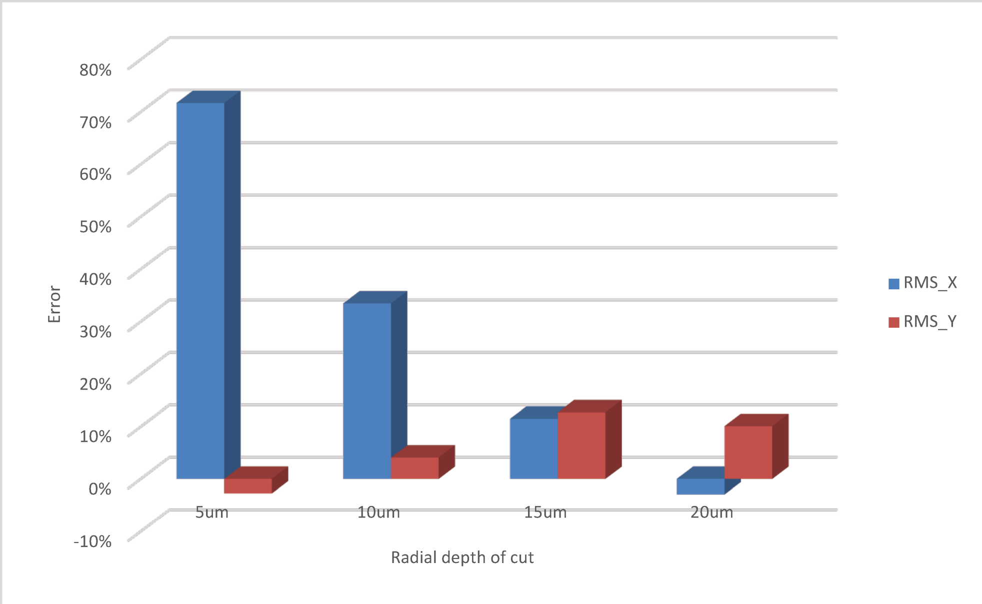

(a)

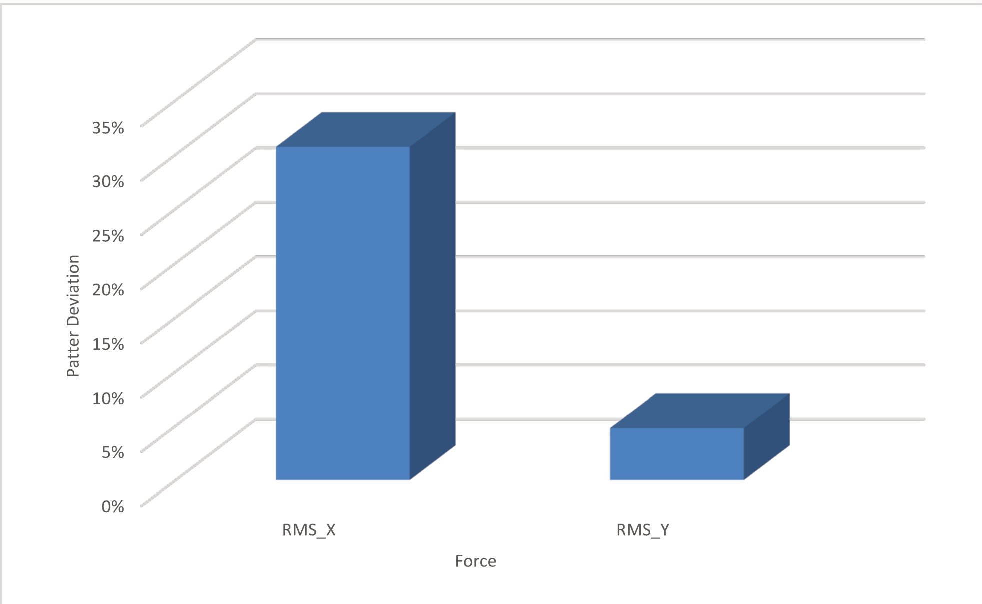

(b)

Finally, a Pattern Standard Deviation (PSD) was used to express the level of dispersion of the data set analyzed, as shown in Figure 17(b). The RMS values of forces at x did not remain uniform because of the high variation of it (31%). The PSD value of x-axis forces was relatively high compared to the y-axis RMS PSD. The results of the RMS values of y-axis forces had 5% of dispersion, and it resented more reasonable values.

5 CONCLUSIONS

The creation of a new method for generating a mesh with realistic geometries of the microstructures of different types of materials from a two-dimensional image was carried out successfully. This makes the method very applicable to study micro behaviors, primarily when it was understood that the microstructure could influence the machining process. The creation of this new method solves the limitation of human interference in the process, thus, guaranteeing better results at the end of the analysis. Another limitation that was overcome was that this method simplified the extraction process of the microstructure for the analysis of finite elements, facilitating the use and dissemination of acquired knowledge.

Furthermore, the effect of workpiece microstructure was studied using finite element analysis. It was seen that the influence of the microstructure in a workpiece in the micro-milling process could affect the results. The x-direction (feed direction) cutting efforts workpiece with microstructure presented 29.75% more than the workpiece without microstructure. However, efforts in y-direction presented values 7.5% higher than in the workpiece without microstructure for the finishing micro-milling process. Therefore, it can be concluded that there will be a high probability of error in the analysis of finite elements in the micro-milling process if the microstructure of the part was not considered.

REFERENCES

AHMADI, M. et al. Microstructure effects on process outputs in micro scale milling of heat treated Ti6Al4V titanium alloys. **Journal of Materials Processing Technology**, v. 252, p. 333–347, 1 fev. 2018.

ARISOY, Y. M. et al. Investigations on microstructural changes in machining of Inconel 100 alloy using face turning experiments and 3D finite element simulations. **International Journal of Mechanical Sciences**, v. 107, p. 80–92, 1 mar. 2016.

ARISOY, Y. M.; ÖZEL, T. Prediction of machining induced microstructure in Ti–6Al–4V alloy using 3-D FE-based simulations: Effects of tool micro-geometry, coating and cutting conditions. **Journal of Materials Processing Technology**, v. 220, p. 1–26, 1 jun. 2015.

BABU, N. K. et al. Influence of microstructure and strengthening mechanism of AlMg5–Al2O3 nanocomposites prepared via spark plasma sintering. **Materials & Design**, v. 95, p. 534–544, 5 abr. 2016.

BARRETT, T. J. et al. An automated procedure for geometry creation and finite element mesh generation: Application to explicit grain structure models and machining distortion. **Computational Materials Science**, v. 141, p. 269–281, jan. 2018.

BREME, H. et al. Chapter 1a Metallic Biomaterials: Introduction. In: **Handbook of Biomaterial Properties**. New York, NY: Springer New York, 2016. p. 151–158.

BROOKES, K. J. A. PM Additive Manufacturing steals the MACH Show. **Metal Powder Report**, v. 69, n. 3, p. 28–32, 1 maio 2014.

BURGER, W.; BURGE, M. J. **Digital Image Processing**. 2 ed ed. London: Springer London, 2016. v. 24

CAMPBELL, A. et al. New methods for automatic quantification of microstructural features using digital image processing. **Materials and Design**, v. 141, p. 395–406, 5 mar. 2018.

CHEN, G. et al. Determination of ductile damage behaviors of high strain rate compression deformation for Ti-6Al-4V alloy using experimental-numerical combined approach. **Engineering Fracture Mechanics**, v. 200, p. 499–520, 1 set. 2018.

CHENG, K.; HUO, D. **Micro cutting : fundamentals and applications**. first ed. [s.l: s.n.].

DECOST, B. L.; HOLM, E. A. A computer vision approach for automated analysis and classification of microstructural image data. **Computational Materials Science**, v. 110, p. 126–133, 1 dez. 2015.

DIETERMANN & HEUSER SOLUTION GMBH. **Professional analysis of the microstructure of cast iron - dhs Solution**. Disponível em: <https://www.dhssolution.com/en/applications/cast-iron-analysis.html>. Acesso em: 8 maio. 2018.

DINIZ, A. E.; MARCONDE, F. C.; COPPINI, N. L. **Tecnologia da Usinagem dos Materiais.** 9. ed. ed. São Paulo: Artliber Editora, 2014.

FRAZIER, W. E. Metal Additive Manufacturing: A Review. **Journal of Materials Engineering and Performance**, v. 23, n. 6, p. 1917–1928, 8 jun. 2014.

GHERMAN, L. et al. Manufacturing Technology: Micro-machining. In: [s.l.] Springer, Cham, 2017. p. 97–127.

GOK, K. et al. Three-dimensional finite element modeling of effect on the cutting forces of rake angle and approach angle in milling. **Proceedings of the Institution of Mechanical Engineers, Part E: Journal of Process Mechanical Engineering**, v. 231, n. 2, p. 83–88, 3 abr. 2017.

GOKHALE, A. M.; YANG, S. Application of image processing for simulation of mechanical response of multi-length scale microstructures of engineering alloys. **Metallurgical and Materials Transactions A**, v. 30, n. 9, p. 2369–2381, set. 1999.

GUEVARA, M. A. et al. Segmentation and Morphometry of Histological Sections Using Deformable Models: A New Tool for Evaluating Testicular Histopathology. In: [s.l.] Springer, Berlin, Heidelberg, 2003. p. 282–290.

JIN, X.; ALTINTAS, Y. Prediction of micro-milling forces with finite element method. **Journal of Materials Processing Technology**, v. 212, n. 3, p. 542–552, 1 mar.

2012.

JOHNSON, G. R. Strength and fracture characteristics of a titanium alloy (. 06al,. 04v) subjected to various strains, strain rates, temperatures and pressures. **Naval Surface Weapons Center NSWC TR**, p. 86–144, 1985.

JOHNSON, G. R.; COOK, W. H. A Constitutive Model and Data for Metals Subjected to Large Strains, High Strain Rates, and High Temperatures. **Proceedings of the 7th International Symposium on Ballistics**, v. 5, p. 541–547, abr. 1983.

KIKINZON, E.; SHASHKOV, M.; GARIMELLA, R. Establishing mesh topology in multi-material cells: Enabling technology for robust and accurate multi-material simulations. **Computers & Fluids**, 29 maio 2018.

KIM, Y.-R.; HAFT-JAVAHERIAN, M.; CASTRO, L. S. Two-Dimensional Virtual Microstructure Generation of Particle-Reinforced Composites. **Journal of Computing in Civil Engineering**, v. 30, n. 1, p. 04014112, jan. 2016.

KOCKS, U. F.; WENK, H.-R.; TOMÉ, C. N. **Texture and anisotropy : preferred orientations in polycrystals and their effect on materials properties**. First ed. New York, NY: Cambridge University Press, 1998.

LANGER, S. A.; FULLER, E. R.; CARTER, W. C. OOF: an image-based finite-element analysis of material microstructures. **Computing in Science & Engineering**, v. 3, n. 3, p. 15–23, 2001.

LEE, Y.-L. et al. Strain-Based Multiaxial Fatigue Analysis. **Metal Fatigue Analysis Handbook**, p. 299–331, 1 jan. 2012.

LJUSTINA, G.; LARSSON, R.; FAGERSTRÖM, M. A FE based machining simulation methodology accounting for cast iron microstructure. **Finite Elements in Analysis and Design**, v. 80, p. 1–10, 2014.

MAHAPATRO, A. Bio-functional nano-coatings on metallic biomaterials. **Materials Science and Engineering: C**, v. 55, p. 227–251, 1 out. 2015.

MATHWORKS. **MATLAB - MathWorks - MATLAB & Simulink**. Disponível em: <https://www.mathworks.com/products/matlab.html>. Acesso em: 14 jun. 2018.

MCNAMARA, G.; DIFILIPPANTONIO, M. J.; RIED, T. Microscopy and Image Analysis. **Current Protocols in Human Genetics**, v. 46, n. 1, p. 4.4.1-4.4.34, jul. 2005.

METALS., A. S. FOR. **Metallography and Microstructures**. 9. ed. [s.l.] ASM International, 2018.

MONTGOMERY, H. C. Method for Measuring Electrical Resistivity of Anisotropic Materials. **Journal of Applied Physics**, v. 42, n. 7, p. 2971–2975, 15 jun. 1971.

NADIMI, S. et al. **A microstructural finite element analysis of cement damage on Fontainebleau Sandstone**. ICTMS. **Anais**...2015Disponível em: <http://openaccess.city.ac.uk/12317/1/ICTMS2015 paper.pdf>. Acesso em: 11 jun. 2018

NICOLETTO, G.; ANZELOTTI, G.; KONEČNÁ, R. X-ray computed tomography vs. metallography for pore sizing and fatigue of cast Al-alloys. **Procedia Engineering**, v. 2, n. 1, p. 547–554, 1 abr. 2010.

NIST. **OOF: Finite Element Analysis of Microstructures**. Disponível em: <https://www.ctcms.nist.gov/oof/>. Acesso em: 11 jun. 2018.

ÖZEL, T.; OLLEAK, A.; THEPSONTHI, T. Micro milling of titanium alloy Ti-6Al-4V: 3-D finite element modeling for prediction of chip flow and burr formation. **Production Engineering**, v. 11, n. 4–5, p. 435–444, 14 out. 2017.

PAN, Z.; FENG, Y.; LIANG, S. Y. Material microstructure affected machining: a review. **Manufacturing Review**, v. 4, p. 5, 23 maio 2017.

PTC. **Creo Parametric 3D Modeling Software | PTC**. Disponível em: <https://www.ptc.com/en/products/cad/creo/parametric>. Acesso em: 19 jun. 2018.

PU, C. L. et al. Effect of microstructure softening events on the chip morphology of AISI 1045 steel during high speed machining. **The International Journal of Advanced Manufacturing Technology**, v. 82, n. 9–12, p. 2149–2155, 17 fev. 2016.

QU, D. et al. Applications of integrated auxiliary methods based on deformation analysis for micro-milling thin-walled slot on micro-neck. **The International Journal of Advanced Manufacturing Technology**, v. 91, n. 5–8, p. 1945–1955, 28 jul. 2017.

RAO, S. S. **The finite element method in engineering**. Sixth ed. [s.l: s.n.].

ROA, J. J. et al. Intrinsic hardness of constitutive phases in WC–Co composites: Nanoindentation testing, statistical analysis, WC crystal orientation effects and flow stress for the constrained metallic binder. **Journal of the European Ceramic Society**, v. 35, n. 13, p. 3419–3425, nov. 2015.

RUSS, J. C. **The Image Processing Handbook**. Sixth ed. New York: CRC Press, 2011. v. 11

SALONITIS, K. et al. Additive manufacturing and post-processing simulation: laser cladding followed by high speed machining. **The International Journal of Advanced Manufacturing Technology**, v. 85, n. 9–12, p. 2401–2411, 17 ago. 2016.

SAMES, W. J. et al. The metallurgy and processing science of metal additive manufacturing. **International Materials Reviews**, v. 61, n. 5, p. 315–360, 3 jul. 2016.

SANTOS, R. G. DOS. **Transformações de fases em materiais metálicos**. Campinas, SP: Editora Unicamp, 2006.

SIMULEON. **Abaqus Tutorials - Perform Non-Linear FEA**. Disponível em: <https://www.simuleon.com/abaqus-tutorials/>. Acesso em: 19 jun. 2018.

TANIMOTO, S. L. **An Interdisciplinary Introduction to Image Processing: Pixels, Numbers, and Programs**. London: MIT Press, 2012.

TESSEMA, A. et al. Effect of filler loading, geometry, dispersion and temperature on thermal conductivity of polymer nanocomposites. **Polymer Testing**, v. 57, p. 101–106, 1 fev. 2017.

THE MATHWORKS, I. **Image Segmentation Using the Image Segmenter App**. Disponível em: <https://www.mathworks.com/help/images/image-segmentation-using-the-image-segmenter-app.html>. Acesso em: 15 jun. 2018.

THEPSONTHI, T.; ÖZEL, T. 3-D finite element process simulation of micro-end milling Ti-6Al-4V titanium alloy: Experimental validations on chip flow and tool wear. **Journal of Materials Processing Technology**, v. 221, p. 128–145, 1 jul. 2015.

THEPSONTHI, T.; ÖZEL, T. Simulation of serrated chip formation in micro-milling of titanium alloy Ti-6Al-4V using 2D elasto-viscoplastic finite element modeling. **Production Engineering**, v. 10, n. 6, p. 575–586, 13 dez. 2016.

VINSON, J. R.; SIERAKOWSKI, R. L. **The behavior of structures composed of composite materials**. [s.l.] M. Nijhoff, 1986.

VINSON, J. R.; SIERAKOWSKI, R. L. **The Behavior of Structures Composed of Composite Materials SOLID MECHANICS AND ITS APPLICATIONS**. 2nd. ed. Dordrecht: Springer Netherlands, 2002. v. 105

WANG, Z. M.; KWAN, A. K. H.; CHAN, H. C. Mesoscopic study of concrete I: generation of random aggregate structure and finite element mesh. **Computers & Structures**, v. 70, n. 5, p. 533–544, 1 mar. 1999.

WAYALUN, P. et al. Images Enhancement of G-band Chromosome Using histogram equalization, OTSU thresholding, morphological dilation and flood fill techniques. **Computing and Networking Technology (ICCNT), 2012 8th International Conference on**, p. 163–168, 2012.

WENK, H.-R.; HOUTTE, P. VAN. Texture and anisotropy. **Reports on Progress in Physics**, v. 67, n. 8, p. 1367–1428, 1 ago. 2004.

YANG, M. et al. New algorithms for virtual reconstruction of heterogeneous microstructures. **Computer Methods in Applied Mechanics and Engineering**, v. 338, p. 275–298, 15 ago. 2018.

YOON, H.-S. et al. A comparison of energy consumption in bulk forming, subtractive, and additive processes: Review and case study. **International Journal of Precision Engineering and Manufacturing-Green Technology**, v. 1, n. 3, p. 261–279, 14 jul. 2014.

ZHOU, J. et al. Realistic microstructural RVE-based simulations of stress–strain behavior of a dual-phase steel having high martensite volume fraction. **Materials Science and Engineering: A**, v. 630, p. 107–115, 10 abr. 2015.

ZHU, J. FEI et al. Real microstructure-based simulation of thermal residual stresses in cemented carbides and the related strengthening and toughening consideration. **International Journal of Refractory Metals and Hard Materials**, v. 71, p. 239–245, 1 fev. 2018.

ZHU, Z. et al. A review of hybrid manufacturing processes – state of the art and future perspectives. **International Journal of Computer Integrated Manufacturing**, v. 26, n. 7, p. 596–615, jul. 2013.